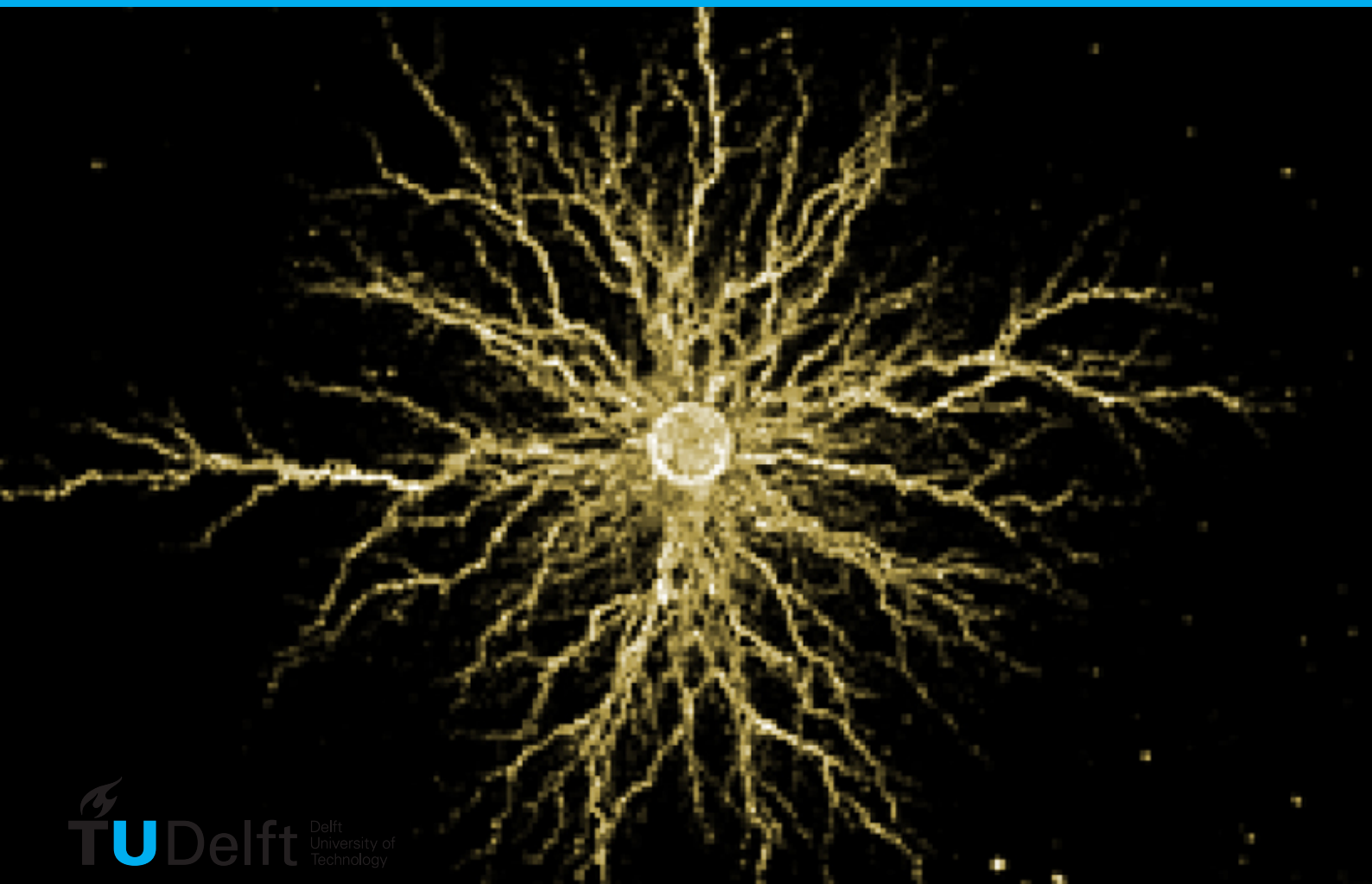


MODELLING OF NEAR-WELL ACIDISATION

ABDUR RAHMAN SHAIK

Masters Thesis
Petroleum Engineering
and Geosciences



MODELLING OF NEAR-WELL ACIDISATION

by

ABDUR RAHMAN SHAIK

to obtain the degree of Master of Science
at the Delft University of Technology,
to be defended publicly on Friday, 17th November, 2017 at 04:00 PM.

Student number: 4511476

Thesis committee: Dr. D.V. Voskov, TU Delft, supervisor
Dr. P. Tomin, Stanford University, supervisor
Prof. Dr. W.R. Rossen, TU Delft
Prof. Dr. G. Bertotti, TU Delft

Cover image courtesy : ExxonMobil

An electronic version of this thesis is available at
<http://repository.tudelft.nl/>.

Contents

List of Figures	v
List of Tables	vii
1 INTRODUCTION	1
1.1 Literature review	1
1.2 Modelling of acidisation	2
1.3 Research goals	5
2 GOVERNING EQUATIONS	7
2.1 Conservation of species	7
2.2 Momentum balance	8
2.3 Chemical reactions	9
2.4 Constitutive relations for porosity and permeability	9
3 SINGLE WORMHOLE PROPAGATION	11
3.1 Discretisation of the governing equations	11
3.2 Simulation results	13
3.3 Conclusive remark	15
4 VALIDATION OF 2D MODEL	17
4.1 Cohen’s simulation model	17
4.2 Validation against Cohen’s model	17
4.3 Comparison with DBS model	19
4.4 Comparison with 1D results	19
5 NUMERICAL CONVERGENCE STUDY	23
5.1 Effect of resolution on capturing the phenomenon	23
5.2 Pore Volumes for Breakthrough (PVBT) analysis	25
5.3 Convergence of the wormhole length	27
5.4 Nonlinear performance analysis	29
5.5 Conclusive remarks	29
6 SENSITIVITY STUDY	31
6.1 Representation in dimensionless numbers	31
6.2 Effect of confinement on wormhole formation	32
6.3 Effect of heterogeneity	33
6.4 Two phase modelling of acidisation : CO ₂ co-injection	35
7 CONCLUSIONS AND FUTURE WORK	39
A APPENDIX	41
A.1 Convergence study with resolution : Relative Error	41
A.2 Exhaustive comparison of Darcy and DBS results	42
Bibliography	43

List of Figures

1.1	(a) Acid Stimulation of an hydrocarbon field. (b) A closer look at the complex dendrite shaped wormholes around a well. Adapted from [1].	2
1.2	(a) Direct Numerical Simulation(DNS) modelling of a typical porous media (b) Volume averaged porosity mapping in Darcy/Continuum modelling.	4
2.1	Schematic of a reservoir with open channel (red), porous region (cyan) and both (yellow).	9
3.1	Flowchart for Darcy model simulation of carbonate acidisation	11
3.2	Changing dissolution front for increasing α i.e. reaction dominating advection.	14
3.3	Growth of wormhole in 1D domain with increasing time - porosity evolution	14
3.4	Growth of wormhole in 1D domain with increasing time - pressure curves.	15
4.1	Fine scale heterogeneous permeability field of 1 mD + 5% with a resolution of [100x160] cells.	18
4.2	Darcy model simulations with AD-GPRS. Wormhole dissolution patterns for increasing injection velocity: (a) Compact Dissolution; (b) Conical Wormhole; (c) Dominant Wormhole; (d) Ramified Wormhole.	18
4.3	Wormhole dissolution patterns for increasing injection velocity. The red field represents region with 100% porosity. The resolution is 200 x 800 cells. Reprinted from [2].	19
4.4	DBS model simulations with AD-GPRS. Wormhole dissolution patterns for increasing injection velocity: (a) Compact Dissolution; (b) Conical Wormhole; (c) Dominant Wormhole; (d) Ramified Wormhole.	20
4.5	Darcy model - Dominant Wormhole dissolution patterns for increasing time. <i>Top</i> : Porosity profiles ; <i>Bottom</i> : Pressure profiles for the times $T = 0.25T_{BT}$, $T = 0.5T_{BT}$, $T = 0.75T_{BT}$ and $T = 0.9T_{BT}$	21
4.6	1D results obtained from the cross-section marked in 4.5. <i>Left</i> : Porosity profiles; <i>Right</i> : Pressure profiles for the times $T = 0.25T_{BT}$, $T = 0.5T_{BT}$, $T = 0.75T_{BT}$ and $T = 0.9T_{BT}$	21
5.1	Darcy model - Conical wormhole at same 0.55 PVI for (a) Very Coarse [25x40], (b) Coarse [50x80], (c) Fine [100x160], (d) Very Fine [200x320] ($Q = 1.6 \cdot 10^{-4}m^3/day$).	24
5.2	DBS model - Conical wormhole at same 0.55 PVI for (a) Very Coarse [25x40], (b) Coarse [50x80], (c) Fine [100x160], (d) Very Fine [200x320] ($Q = 1.6 \cdot 10^{-4}m^3/day$).	24

5.3	PV_{BT} decline with the increasing number of grid cells obtained for simulations in ADGPRS for ramified wormhole. DBS model was employed.	25
5.4	PVBT analysis for different resolutions. Left: Darcy model, Right: DBS model.	26
5.6	Porosity maps for the evolution of wormholes for changing velocity - Darcy model.	26
5.5	PVBT analysis comparison of Darcy and DBS for a resolution of [100x160].	27
5.7	Ratio of length of the leading wormhole to the length of the average wormhole for (a) Darcy model (b) DBS model.	28
5.8	Comparison of ratio of length of the leading wormhole to the length of the average wormhole for Darcy and DBS models for a resolution of [100x160].	28
5.9	Time steps statistics comparison for as simulation time of 0.01 days for different timesteps. <i>Left</i> : Darcy model ; <i>Right</i> : DBS model	29
5.10	Newton Iterations statistics comparison for as simulation time of 0.01 days for different timesteps. <i>Left</i> : Darcy model ; <i>Right</i> : DBS model	29
6.1	Analysis of PVBT with changing Damkohler number	32
6.2	Analysis of PVBT with changing Peclet number	32
6.3	DBS model - Wormholes formation in (a) unconfined condition with a height of 0.4 m (b) confined conditions with height of 0.1 m (c) confined with 0.05 m height	33
6.4	Wormhole growth in the Darcy (left) and DBS (right) models for different confinement ratios.	33
6.5	Porosity maps for Darcy model for permeability perturbation of 5% 10% and 20% showing several dominant wormholes.	34
6.6	Porosity maps for DBS model for permeability perturbation of 5% 10% and 20%.	34
6.7	Wormholing dynamics for Darcy (left) and DBS (right) models for permeability perturbation of 5% 10% and 20%.	35
6.8	PVBT analysis of two phase and comparison with single phase with Darcy model.	36
6.9	PVBT analysis of two phase and comparison with single phase with DBS model.	36
6.10	Smearing and retardation of wormholes due to CO_2 co-injection. a) Porosity field of conical wormhole b) CO_2 concentration around wormhole.	36
A.1	Relative Error % in PVBT for (a) Darcy model (b) DBS model relative to the [200x320] solution.	41
A.2	PVBT analysis comparison of Darcy (left) and DBS (right) for a resolutions of top :[25x40] [50x80] , bottom : [100x160] [200x320]	42
A.3	Comparison of ratio of length of the leading wormhole to the length of the average wormhole for Darcy and DBS models.	42

List of Tables

4.1	Simulation parameters used for acid stimulation modelling	18
5.1	Comparison of numerical and physical diffusion coefficients.	25

ABSTRACT

Acidisation is one of the oldest techniques of enhancing oil recovery, going back more than a 100 years ago. The accurate description of this physical and chemical phenomenon is not a straightforward task. The Darcy law, which is commonly used in *continuum modelling* at macroscale, fails when the porosity approaches the unity due to a dissolution. In order to accurately capture the acidisation phenomenon, an upscaling of Navier-Stokes equations is done from pore scale to Darcy scale. The resulting equation is called the Darcy-Brinkman-Stokes (DBS) equation and the approach is called *hybrid modelling*. The hybrid modelling has the advantage of not having to deal with jumps in velocity and pressure as it makes these variables continuous without any jumps at the interfaces.

The research presented here models the phenomenon using both the Darcy and DBS approaches to study the differences. A single phase injection model in 1-D is simulated to understand the flow dynamics and the chemical kinetics of a single wormhole in idealistic assumptions. To study different regimes of wormholes formation, the 2-D model, implemented in Stanford's Automatic Differentiation General Purpose Research Simulator (ADGPRS), was employed. The shape of wormholes is studied and is validated against the published results. The wormholes characteristics, obtained in both Darcy and DBS models, are defined as a function of breakthrough parameters and dimensionless variables. A convergence, sensitivity and performance analysis is performed for key parameters to fully describe and understand the differences in the 2-D solutions. Furthermore, the impact of co-injecting a gas phase namely CO₂ is simulated and compared with the single phase injection in both the models.

ACKNOWLEDGEMENT

My first and the biggest gratitude is towards my supervisor Dr. Denis Voskov who had faith in me from the start and guided me through the end with extreme patience, intellect and professionalism, unmatched by any of my teachers throughout my years of education. I am greatly indebted to Dr. Pavel Tomin of Stanford University for helping me deal with simulation issues and counsel more times than I can count while being in a completely different time-zone. His resolve to help, patience and humility inspires all the students who had the opportunity to meet him. I would also like to thank Prof. Rossen for being such an inspiration to us all and always treating students with an extra bit of empathy and understanding. His SPE article 'Should I Consider Graduate School?' is a fantastic read and it got me here to TUD. My sincere gratitude also goes out to Dr. Hadi Hajibeygi, whose coursework on Reservoir Simulation inspired me to take up my research in that direction. It was an honour to learn from these exceptional teachers.

I am greatly thankful to the Stanford University Reservoir Simulation Research program (SUPRI-B) for letting me use the Automatic Differentiation General Purpose Research Simulator (AD-GPRS) for my thesis research. I would also like to thank Mark Khait for helping me initially setup ADGPRS and several more times with cluster.

My thanks goes out to my fellow MSc classmates whose presence, advice and discussion have had a strong positive impact on my thesis, making the experience a very happy one. Special thanks goes to my friends Ravi, Abby, Ali for making my time in Netherlands so far an amazing experience. My friends back at home from BITS-Pilani also offered great support while I was here. My classmates and I are grateful to Margot Perk of CiTG for shielding us from the paperwork and helping us file for graduation in time.

Finally, I would like to dedicate my thesis as an expression of gratitude to my parents, who sacrificed their all for my few. Ammi and Baba, you inspire me.

*Rahman Shaik
Delft, August 2017*

INTRODUCTION

1.1. Literature review

The near-well area is the most accurately characterised region of the subsurface porous media. Most logging tools capture the data such as porosity, resistivity, density, sonic time up to a high degree of accuracy, hence making the near borehole area well distinguished. This detailed description can be used for an accurate study of different processes related to well productivity. Based on these studies, we can predict and further optimize the performance of the well and in addition propose more accurate models for the large scale representation of well.

One of these processes used to improve well's productivity is a near-well acidising. Acid stimulation is one of the most employed techniques used in subsurface engineering. The first patent for an acid job dates back to 1896 [3], and it is still a widely used industry practice with a century after it was conceived. In 1994, 79% of the stimulation jobs in the petroleum industry were comprised only of acid stimulation [4]. Today, this technology is wildly employed in multiple industrial activities including some geothermal projects [5, 6].

The growing global energy consumption and drive for cleaner energy has generated an immense interest in low enthalpy geothermal energy resources (LEGERs) as an alternative and readily available resource. These resources, albeit under 100°C, can be harvested to provide heating and power generation from household to industrial scale. One of the challenges encountered during the exploration of such geothermal reservoirs is the poor hydraulic connectivity of wells caused by drilling mud. A related and critical challenge is the natural precipitation of rock which leads to a permeability reduction i.e. formation damage in the near-well area. Although hydraulic stimulation along the entire reservoir can be applied to improve the efficiency of such wells, the application of chemical stimulation to the near-well region can also be effective without risks posed by fracking. There are strong similarities between hydrocarbon and low enthalpy geothermal reservoirs in terms of extraction, injection and well optimisation methods including matrix acidising [7, 8].

Another reason why the study of the near-well area is of considerable importance is its impact on the overall pressure profile during extraction. In a radial flow well, the first 20 ft accounts for 50% flowing pressure gradient drop and just the first 3 ft account for 25% of it. If these near well areas are affected by formation damage, it could have a pronounced effect on well performance [9]. To remove formation damage

due to clogging of the pores and to restore and improve permeability, acid stimulation is employed. If the acid is injected at a pressure above the fracture gradient, it is called *fracture acidising*. The acid propagates across the face of the fracture and penetrates deep into the reservoir. Another strategy is to pump the acid into the reservoir below the formation pressure so that the acid flows, dissolving the damage through the reservoir via the existing pores and the natural fractures. This strategy is known as *matrix acidising* and it is studied in this report.

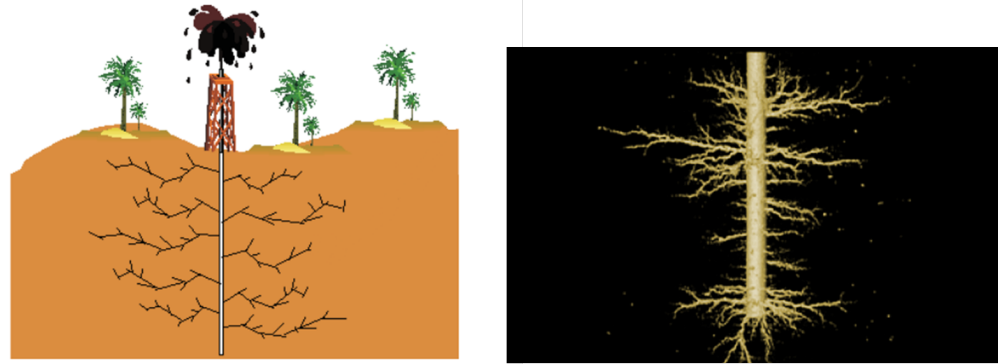


Figure 1.1: (a) Acid Stimulation of an hydrocarbon field. (b) A closer look at the complex dendrite shaped wormholes around a well. Adapted from [1].

1.2. Modelling of acidisation

The modelling of acid stimulation depends heavily on how the flow properties are handled in the solution. The physics of transport needs to be solved accurately and on sufficient scale to model the system. The chemical description of the species, the mineral-fluid reactions and their impact on the the physical model is of great interest when it comes to acidising. The chemical species have several reversible and mutually non-exclusive reactions which alter the rate of the reaction. The thermodynamics of the reactions has an impact on the chemical equilibrium of the species. Therefore, the complex chemical thermodynamics and equilibria of these species need to be handled well in a three-phase system of solid, liquid and gas. Although several species and mutual interactions help to model the system accurately, it leads to a rigid and complex solution. A wise choice of the key phenomena and simplification of model without losing any resolution or accuracy also needs to be made a priority.

The main purpose of modelling the acid stimulation is to study the evolution of *wormholes*. Wormholes are channels of dissolved carbonate rock with porosity close or equal to 1. In the modelling process, they can be introduced as high permeability channels for improved flow of fluid to the production tubing. When the acid is injected at a very slow rate, the penetration is not effective. Extremely high rates of injection lead to fracking and are not effective as the residence time is not enough for the acid to react with the matrix. Hence, intermediate flow rates are desired. At the optimum rates, the wormholes shape is ideal because the acid is spent for prolongation of very few dominating wormholes [10]. Accurate representation of these wormholes is paramount in developing the simulation model of the acidisation process. There are generally two approaches to model a flow problem in porous media namely *Darcy scale* approach and *pore-scale* approach.

In 1856, Henry Darcy published his work on water flow in a sandpack which later became known as the famous Darcy's law [11]. This law is a great tool while dealing with any flow in the porous media but it has its shortcomings, specifically, when it comes to representing reactive fluid transport in CO₂ sequestration [12, 13] where the permeability is low and the micro-scale flow model is complex. Similarly, Darcy's law fails to model the system accurately in the case of dissolution when the porosity of the grid cells is high and nearly 100%. Moreover, modelling of a moving solid-fluid boundary with Darcy's law is a challenging task.

In the pore scale model, the porous media is explicitly defined. The pore and pore-throat are resolved separately as an object with either the Stokes or Navier-Stokes' equation. This can be seen as the solution of these equations for a flow past irregular objects at a small scale. This approach is understandably intensive and difficult to perform without exact mapping of the porous medium at high resolution. The practical problems at field scale require a large volume of rock mapping. This approach, although direct, is not so practical to apply for large scale problems. Hence this pore-scale is called *Direct Numerical Simulation* (DNS) or *Micro-scale modelling* [14]. For this micro-scale modelling, the momentum equation for single-phase flow i.e. the Stokes equation (subset of Navier-Stokes' equations) is given by

$$\nabla P - \mu \Delta \vec{V} = 0, \quad (1.1)$$

where P is the fluid pressure, \vec{V} the velocity, and μ the viscosity. The Darcy scale modelling relies on an average definition of properties. Instead of explicitly resolving the millions of pores and pore-throats, Darcy scale model breaks it down to a limited number of elementary volumes with a variable flow properties such as *porosity* (volume fraction of solids) and *permeability*. Using these average properties, the canonical Darcy's law can be used to solve the flow problem. Since we translate information from a very small scale to the Darcy scale, this approach is also called *Continuum modelling* or *Macro-scale modelling*. Figure 1.2 illustrates the two ways of modelling.

For the macro-scale, the momentum equation, based on a volume average approach (denoted by $\langle \cdot \rangle$), is given by the Darcy's law:

$$\nabla \langle P \rangle + \frac{\mu}{K} \langle \vec{V} \rangle = 0, \quad (1.2)$$

where K is the permeability. The second term in the equation describes the dissipative momentum loss due to solid-fluid interactions.

Most of the existing research work on carbonate acidising has been done with a Darcy approach [1, 2, 10, 15]. While being quite useful for understanding the wormhole formation, these approaches do not capture all dissolution phenomenon at high fidelity. In particular, the Darcy model is more appropriate for a macro-scale simulation and it is not completely sufficient in situations where the (averaged) porosity is approaching 1. An accurate upscaling of pore-scale equations from the micro-scale to the macro-scale scale or multiscale approaches (e.g. [16–18]) should ideally resolve this issue. It is first proposed by Brinkman [19] that the equation capable to bridge the two scales should be reflected by Darcy's law with an additional term $\mu' \Delta \vec{V}$ which he motivated purely by a mathematical consideration that it is impossible to pose a boundary condition between the first order Darcy's equation and

second order Stokes' equation. This additional term comes directly from the Stokes equation and physically it describes the viscous shearing stresses acting on a volume element of fluid. The viscosity coefficient, μ' , can be different from the true fluid viscosity, μ .

The resulting equation is called the Darcy-Brinkman-Stokes (DBS) equation and can be written as

$$\nabla\langle P\rangle + \frac{\mu}{K}\langle\vec{V}\rangle - \mu'\Delta\langle\vec{V}\rangle = 0. \quad (1.3)$$

The advantage of this model is that it converges to the Darcy's law in the control volumes with low permeability and resolves to the Stokes' equation in control volumes with very high permeability. This approach introduces a diffusive layer between solid and void domains and effectively handles the velocity jump which needs to be resolved in other approaches (e.g. a two-domains approach). This modelling method is aptly referred to as the *hybrid modelling* or *micro-continuum modelling*. This hybrid model henceforth is a primary simulation tool used in this research work.

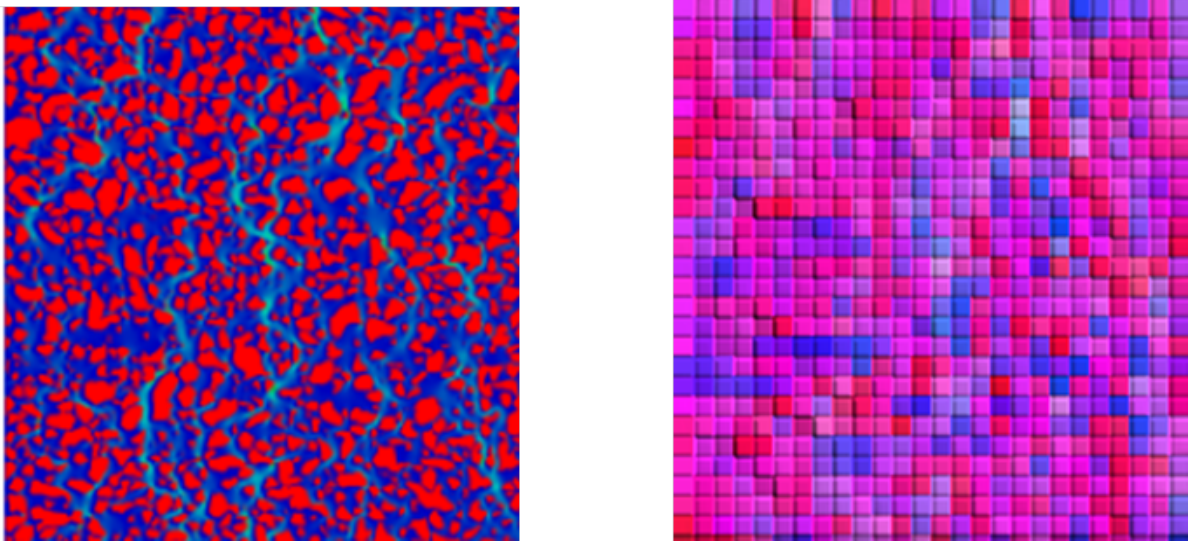


Figure 1.2: (a) Direct Numerical Simulation (DNS) modelling of a typical porous media (b) Volume averaged porosity mapping in Darcy/Continuum modelling.

1.3. Research goals

In this thesis, we study the acidisation phenomenon using a micro-continuum approach with hybrid modelling. The main focus is to understand the difference introduced by DBS approach in comparison to the classic Darcy model and if these differences are significant enough to prefer the more computationally expensive approach of DBS.

First, a simple 1D model of a reservoir with constant acid injection is simulated using Darcy model in MATLAB to understand the governing equations and to check if this set-up is sufficient to study the phenomenon of acidisation. An incompressible flow with a first order reaction, controlled by the rate of convection, is taken in the starting model. While this tool is capable to address some questions related to acidising process, it is not sufficient enough to model wormholes.

That is why we employ both the Darcy and DBS models developed in Stanford's Automatic Differentiation General Purpose Research Simulator (ADGPRS) [20–26]. The momentum equation is solved using the Darcy-Brinkman-Stokes equation. Parameters such as resolution, Damkohler number (Da), Peclet (Pe) are analysed in order to measure the impact of reaction, convection, and diffusion time. The injection rates are changed to study the types of wormhole formed and their breakthrough time. The breakthrough pore volume (PV_{BT}) is used to measure the volumes of acid needed for the wormholes to reach the boundary of the domain. A study on the impact of heterogeneity and confinement is also performed to measure the effect on the breakthrough time and the type of dissolution pattern. Finally, the impact of gas co-injection is simulated and compared with the single phase injection.

2

GOVERNING EQUATIONS

In the present challenge to predict the acidisation and to optimise the acid-job for the entire formation, it is fortunate that studying the near well area and its characterising helps us to predict the acidisation growth along the formation. Hence, the thesis is titled, focusing on modelling of the near-well zone. This section elucidates the modelling approach employed in the developed MATLAB code and the model, implemented in Automatic Differentiation General Purpose Research Simulator (ADGPRS), developed by the SUPRI-B research group at Stanford University. The governing equations for reactive transport involve a combination of mass conservation, kinetic reaction model for chemical species, and momentum conservation. A two-phase model of solid (s) and fluid phase (f) is considered with water, acid, reaction product, and solid components. Molar variable formulation is used to solve the governing equations, as described in [21]. The coupled system of equations is spatially discretised employing a finite-volume scheme with a two-point flux approximation. The non-linearities are handled using Newton's method and the resulting linear matrix system is solved using the Parallel Sparse Direct Solver (PARDISO) [27].

2.1. Conservation of species

General form of the mass conservation equation for i^{th} fluid component is given by

$$\frac{\partial}{\partial t} \left(\phi \sum_{j=1}^{j=N_p} x_{ij} \rho_j S_{ij} \right) + \nabla \cdot \sum_{j=1}^{j=N_p} \left(x_{ij} \rho_j \vec{V}_j - \phi \rho_j S_j D_{ij} \nabla x_{ij} \right) = \sum_{k=1}^{k=N_r} \nu_{ik} r_k \quad (2.1)$$

where the variables are:

- x_{ij} = Mole fraction of i^{th} component in j^{th} phase
- ρ_j = Molar density of j^{th} phase
- S_j = Saturation of j^{th} phase
- D_{ij} = Diffusion coefficient tensor
- V_j = Velocity of j^{th} phase
- ν_{ik} = Stoichiometric coefficient of i^{th} component in k^{th} reaction

- r_k = Reaction rate of k^{th} reaction

(N_p is the number of phases, N_r is the number of reactions.)

The solid species is dissolved into the liquid phase and the solid concentration decay can be accounted as

$$\frac{\partial C_s}{\partial t} = \sum_{k=1}^{j=N_r} v_{sk} r_k \quad (2.2)$$

where C_s is the solid concentration over the control volume. Note that the fluid component concentrations are defined over the net fluid (= pore) volume and the solid concentration is defined over the entire control volume which includes fluids + solids.

2.2. Momentum balance

Usually the relationship between pressure and velocity is given by the canonical Darcy's law [11]. The velocity of the j^{th} phase is given by

$$\vec{V} = -\frac{K}{\mu} \nabla P. \quad (2.3)$$

The key difference between the Darcy model and the Darcy-Brinkman-Stokes (DBS) model is the handling of control volumes with high porosity. Since it is incorrect to apply Darcy's Law in regions with near 100% porosity, the simulation model obtained with Darcy's is therefore not as accurate as the Stokes' model used for an open channel flow. One way to avoid this shortcoming is to allocate regions with high porosity and apply Stokes' equations there when Darcy's law can be applied elsewhere. However, this approach requires some correction to the boundary of these regions to preserve continuity.

Instead, one can employ the Darcy-Brinkman-Stokes' (DBS) equation. It is a unified, single continuum approach that is valid for the described problem since it inherently takes into account the amount of open channel and porous media in the control volume. The DBS equation is given by

$$\nabla P + \frac{\mu}{K} \vec{V} - \frac{\mu}{\phi} \Delta \vec{V} = 0 \quad (2.4)$$

The third term in the equation is the dissipative viscous forces encountered in the free channel. In contrast to the Stokes' equation, the viscosity is no longer μ but an effective viscosity given by μ/ϕ . The fluid does not have its original viscosity on account of momentum dispersion as reported by Liu and Masliyah [28] (chapter 3, page 100). Although there is no clear consensus on the application of effective viscosity [29], numerical simulations done by Ochoa-Tapia and Whitaker [30] confirm that the effective viscosity is indeed increased by a multiplier of $1/\phi$. Hence, this modification was done to the Brinkman equation consistent with other experimental and simulation works [13, 31–36]. Consider the application of the above equation to the control volumes shown in 2.1:

- In the **red** control volume, there is no porous medium present and hence the Stokes' equation can be applied to calculate the pressure drop. Here, the DBS equation is valid too, as the second term, $\frac{\mu}{K} \vec{V}$, becomes zero as there is no flow resistance in the open channel ($K \rightarrow \text{inf}$).

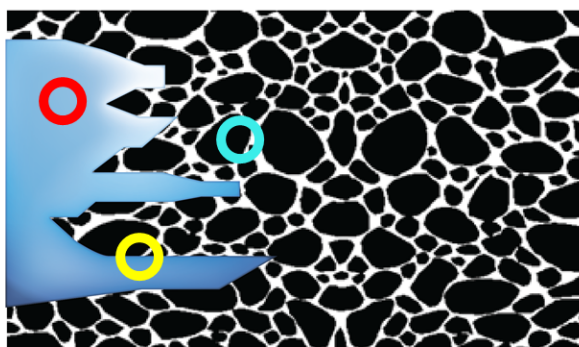


Figure 2.1: Schematic of a reservoir with open channel (red), porous region (cyan) and both (yellow).

- In the cyan control volume, the entirety is filled with porous medium and we can use the classic Darcy's law. In the DBS equation, the third term, $-\frac{\mu}{\phi}\Delta\vec{V}$, becomes insignificant in comparison to the dominating flow resistance term.
- In the yellow control volume, the boundary between porous media and void is present. This problem is solved with the single continuum equation with accounts for both the flow resistance and dissipative viscous forces proportional to the porosity.

2.3. Chemical reactions

The chemical reaction is assumed to be a simple first order kinetic reaction consistent with dissolution of rock with acid



where the reaction rate is given by

$$r = \alpha C_s z_{acid}. \quad (2.5)$$

Here α is the reaction rate constant and z_{acid} is the acid concentration.

2.4. Constitutive relations for porosity and permeability

The distinctive feature of reactive transport in comparison with normal single phase flow is that the porosity and permeability fields are no longer constant and must be updated as the acid dissolves the carbonate matrix. This porosity increase has a direct relationship with the remaining amount of solid concentration left, which is given by

$$\phi_0 = \phi_0^{init} + (v_{s0} - v_s), \quad (2.6)$$

where $v_s = \sum C_s v_s^m$ is the volumetric fraction of solid concentration in the control volume and v_{s0} is the initial volumetric fraction the solid (v_s^m is the molar volume). The difference between v_s and v_{s0} address the amount of solid volumetric fraction dissolved i.e. the amount of porosity increase in the control volume.

The updated values of ϕ_0 are used to update the porosity field due to the pressure change

$$\phi = \phi_0 [1 - c_r(p - p_{\text{ref}})], \quad (2.7)$$

where c_r is the formation compressibility factor, p the pressure in the control volume, p_{ref} the reference pressure.

Since it is well established that porosity and permeability are strongly related and there exist several poro-perm relationships, we need to apply one such relationship to update the permeability field after the deposition of solid. In this study, we employ a Kozeny-Carman relationship [37, 38] for this update

$$\frac{K}{K_0} = \frac{\phi^3(1 - \phi_0)^2}{(1 - \phi)^2\phi_0^3}, \quad (2.8)$$

where K and K_0 are the current and initial permeabilities, respectively.

SINGLE WORMHOLE PROPAGATION

The starting point of our study is related to the better understanding of the wormhole phenomenon and its sensitivity. As the first step towards this goal we are using a 1D dissolution model which describes an idealistic propagation of a single uniform wormhole. The general governing equations (2.1,2.2,2.3) are presented here in a simplified form, discretised and solved sequentially in a MATLAB code with the assumption of a single phase incompressible Darcy flow under isothermal conditions.

3.1. Discretisation of the governing equations

The discretised model was initially solved in MATLAB code using IMPEC (Implicit Pressure Explicit Concentration) approach. The overall scheme, describing the solution procedure, is shown in Fig. 3.1.

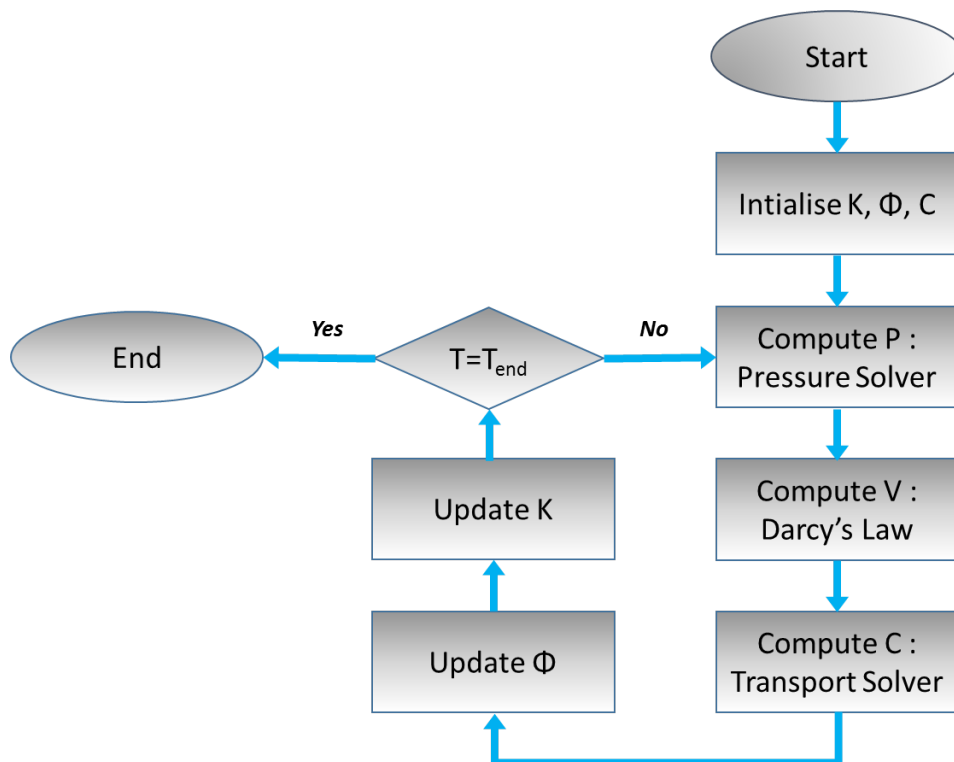


Figure 3.1: Flowchart for Darcy model simulation of carbonate acidisation

Step 1: Pressure solver For an incompressible flow, the mass conservation of a i^{th} species in ω^{th} phase is given by

$$\phi \frac{\partial S_\omega}{\partial t} - \nabla \cdot (\lambda_\omega \nabla p) = q_\omega. \quad (3.1)$$

Where S_ω is the saturation of ω phase, p is pressure, λ_ω is the mobility and q_ω is the source term.

The total pressure equation can be obtained by summing up the mass conservation equation for each component. The summation of equation 3.1 over all the phases leads to -

$$-\nabla \cdot (\lambda \nabla p) = q. \quad (3.2)$$

Where λ is total mobility and q is the source term.

This equation can be discretised using the finite difference method and written for cell i to obtain

$$\frac{\left(-\lambda \frac{\partial p}{\partial x}\right)^{i+\frac{1}{2}} - \left(-\lambda \frac{\partial p}{\partial x}\right)^{i-\frac{1}{2}}}{\Delta x} = q_i, \quad (3.3)$$

$$\left(-\lambda \frac{\partial p}{\partial x}\right)^{i+\frac{1}{2}} = -\lambda_t^{i+\frac{1}{2}} \frac{p_{i+1} - p_i}{\Delta x}. \quad (3.4)$$

Where $\lambda_t^{i+\frac{1}{2}}$ is the harmonic averaged mobility at the interfaces of cell i and $i+1$ and Δx is the grid size.

Substituting equation 3.4 in equation 3.3 reduces the pressure solution to a linear system of the form $\mathbf{A}p = \mathbf{q}$ which can be solved to obtain the pressure solution.

Step 2: Velocity solver After the pressure in each grid cell is obtained, the velocity (flux) is obtained using the Darcy's law:

$$\vec{V}_{i+\frac{1}{2}} = -\lambda_t^{i+\frac{1}{2}} \left(\frac{p_{i+1} - p_i}{\Delta x} \right). \quad (3.5)$$

Where $\vec{V}_{i+\frac{1}{2}}$ is the velocity on the interface between cells i and $i+1$

Step 3: Transport solver The general advection-diffusion equation with reactive transport is given by

$$\frac{\partial (\phi C)}{\partial t} + \nabla \cdot (\vec{V} C) - \nabla \cdot (\phi D \nabla C) = -\alpha C. \quad (3.6)$$

Where C is the concentration of the species, α is the reaction rate constant, \vec{V} is the velocity, ϕ is the porosity and D is the effective Dispersion tensor. Assuming porosity is constant during the timestep Δt , the equation reduces to

$$\phi \frac{\partial C}{\partial t} + \nabla \cdot (\vec{V} C) - \phi D \nabla \cdot (\nabla C) = -\alpha C. \quad (3.7)$$

Solving the equation 3.7 explicitly and using upwind approximation for the second term for i^{th} grid cell, the concentration for the grid cell becomes

$$C_i^{n+1} = \frac{C_i^n \left(\frac{\phi_i}{\Delta t} - \alpha - \frac{2D\phi_i}{\Delta x^2} - \frac{\tilde{v}_{i+\frac{1}{2}}^n}{\Delta x} \right) + C_{i-1}^n \left(\frac{\tilde{v}_{i-\frac{1}{2}}^n}{\Delta x} + \frac{D\phi_i}{\Delta x^2} \right) + C_{i+1}^n \left(\frac{D\phi_i}{\Delta x^2} \right)}{\frac{\phi_i}{\Delta t}}. \quad (3.8)$$

Step 4: Porosity update The increase in acid concentration leads to a decrease in the porosity. This change is governed by the equation

$$\frac{\partial \phi}{\partial t} = \frac{v\alpha C_i^n}{\rho_s}. \quad (3.9)$$

Where v is the stoichiometric coefficient, taken as 1 for the reaction and ρ_s is the density of the rock.

The discretisation of the above equation gives the porosity in the cell as :

$$\phi_i^{n+1} = \phi_i^n + \frac{\Delta t v \alpha C_i^n}{\rho_s}. \quad (3.10)$$

Step 5: Permeability update The poro-perm relationship to update the increase in permeability due to increasing porosity is taken from Panga et al. [15]. It is given by

$$K = \left(\frac{\phi}{\phi_o} \right) \exp \left(\frac{b(\phi - \phi_o)}{1 - \phi} \right). \quad (3.11)$$

Where K is the permeability, ϕ_o is the initial porosity and b is a fitting parameter taken as 1.2 in this simulation.

Once the permeability is updated, the pressure solver is now updated with this new permeability field to recompute the pressure profile (step 1), the resulting velocity profile (step 2) and the subsequent changes in porosity and permeability. This process is described in the Fig. 3.1 and is repeated until breakthrough or end of the simulation.

3.2. Simulation results

Here we present the results of the first simulation study, related to the sensitivity of wormhole growth to the reaction rate. The porosity distribution is shown in Fig. 3.3. You can see that the obtained profiles are much steeper than in the case of simple advection-diffusion equation due to the reaction term which dominates diffusion. Hence the fronts are no longer smoothly and steadily declining.

For lower reaction rates i.e. for smaller values of reaction rate constant, α , the porosity field first displays an exponential decline for smaller reaction rates as the reaction time scale is now larger than the flow time scale and there is insufficient time for the incoming acid to dissolve all of the rock. Hence at low acid reaction rate, the porosity at the entrance does not start from 1. On increasing the reaction rate, the acid now has more than sufficient time to dissolve the rock and the porosity field in the initial length of the rock is now 1 as the rock is dissolved in that length. The unconsumed acid going past this dissolved region i.e. the 'wormhole' is less than what is needed to dissolve the rest of the rock and therefore we see a decline in the porosity field.

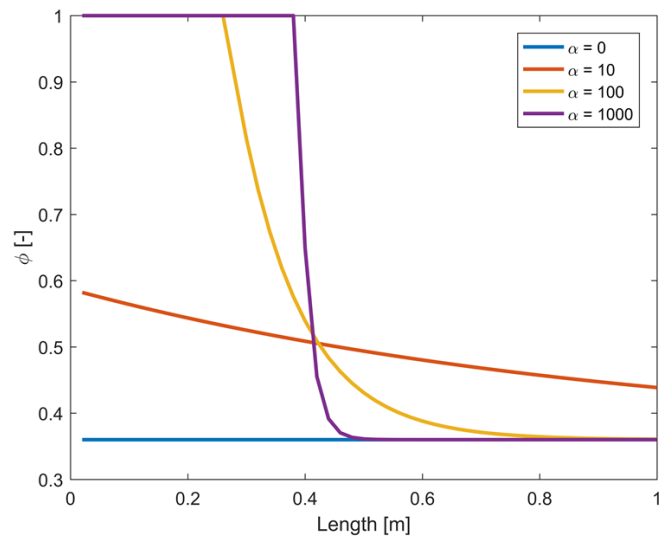


Figure 3.2: Changing dissolution front for increasing α i.e. reaction dominating advection.

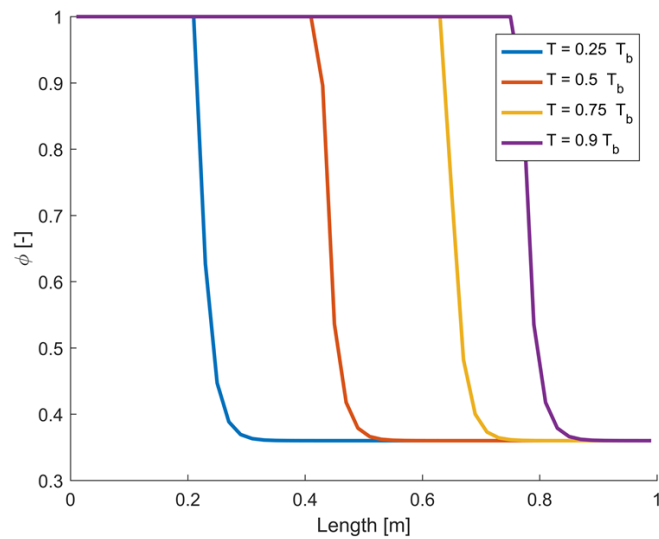


Figure 3.3: Growth of wormhole in 1D domain with increasing time - porosity evolution

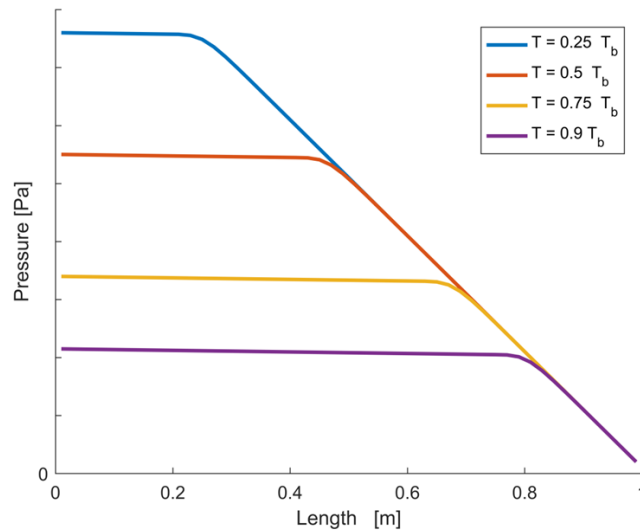
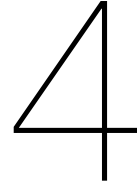


Figure 3.4: Growth of wormhole in 1D domain with increasing time - pressure curves.

3.3. Conclusive remark

While the 1D model seems quite useful for addressing some characteristics of wormhole dynamics, it cannot address the most important question related to the wormholes spatial distribution. In addition, a significant difference between 1D and 2D models has been reported in the past [39]. Because of this, we decided to focus on 2D simulations in our study. Due to the computation limitations of the MATLAB, a simulation model based on both Darcy and DBS approach, implemented in Stanford's ADGPRS framework, will be used in the following sections.



VALIDATION OF 2D MODEL

In this chapter, we adapt the dissolution model developed in AD-GPRS simulator. First, we compare our 2D simulation results with the simulation study performed by Cohen [2]. His study is based on a core-scale non-equilibrium model proposed in [1]. To test the applicability of the model to acid injection, we finally compare it with 1D solution obtained in the previous chapter under idealistic assumptions. In this study, we assume an incompressible flow in the absence of gravity effects.

4.1. Cohen's simulation model

The governing equations used in the work by Cohen et al. [2] are similar to the ones used in the previous chapter to develop the 1D simulator. A first order, irreversible reaction in a heterogeneous reservoir for incompressible flow was modelled under isothermal conditions. The slight difference was in the consideration of effective diffusivity which was taken as ϕD in equation 3.6 is reduced to just D , i.e. making it independent of the porosity. This assumption is valid for low diffusion coefficients, which is the case in the current simulation.

A 2D carbonate block of dimensions 25 x 40 x 0.1 cm is simulated with an injection concentration of $C_{A\beta} = 210 [kg/m^3]$ and stoichiometric coefficient ϑ as 1, for a first order irreversible reaction. The initial porosity of this domain is 0.36. The permeability of the model is 1 mD and a small perturbation of 5% in permeability field is introduced to mimic the micro-scale heterogeneity as shown in the Fig. 4.1. The fluid is injected from the left face at a constant injection rate while the pressure at the downstream boundary is kept constant.

The model in AD-GPRS is solved using a Fully Implicit Method (FIM). The simulation parameters used in the validation and in the simulations that follow in the further chapters are shown in the Tab. 4.1.

4.2. Validation against Cohen's model

With the resolution of [100x160] cells, the following results were obtained with the Darcy model after injecting 0.7 Pore Volumes, as shown in the Fig. 4.2.

As you can see, the results qualitatively reproduce the Cohen model except for few unimportant details. While both conical and ramified regimes look quite similar, the dominant wormhole is more pronounced in Cohen model. We can address these

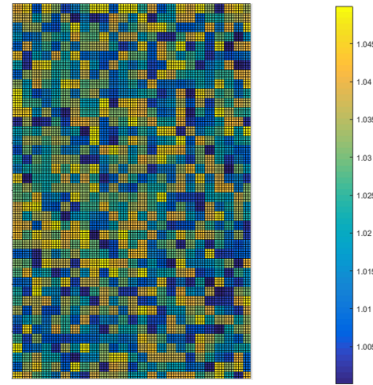


Figure 4.1: Fine scale heterogeneous permeability field of 1 mD + 5% with a resolution of [100x160] cells.

Parameter	Property	Value	Units
K	Permeability	1.0	mD
L_y	Height	0.4	m
L_x	Length	0.25	m
ϕ	Porosity	0.36	-
ΔK	Permeability perturbation	5 %	-
α	Reaction rate constant	10	1/s
$x_{acidini}$	Initial Acid concentration	0.001	-
x_{H_2Oini}	Initial Water concentration	0.997	-
x_{acideq}	Equilibrium Acid concentration	0.1	-
x_{acid}	Concentration of acid in injection	0.7500	
x_{H_2O}	Concentration of Water in injection	0.2498	
P_{BC}	Pressure boundary condition downstream	100	
D	Diffusivity	10^{-9}	m^2/s

Table 4.1: Simulation parameters used for acid stimulation modelling

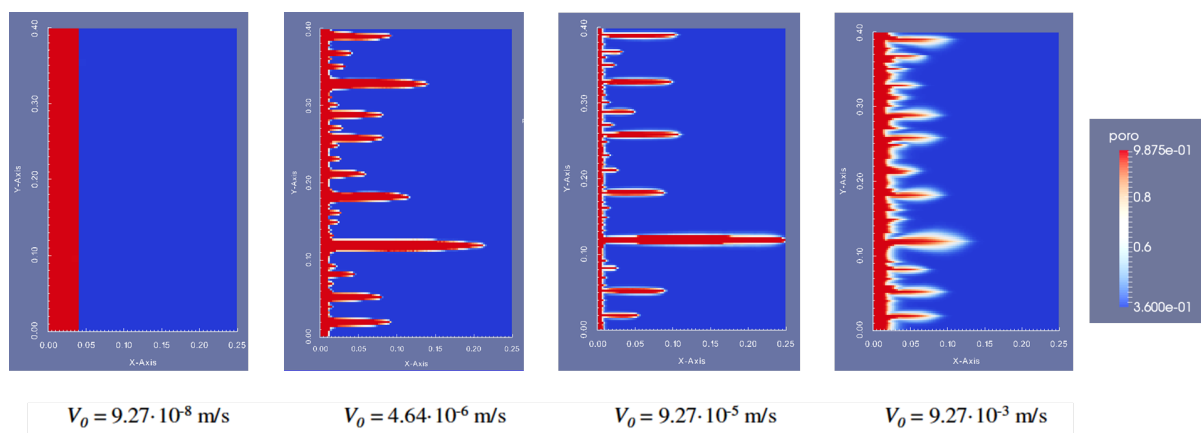


Figure 4.2: Darcy model simulations with AD-GPRS. Wormhole dissolution patterns for increasing injection velocity: (a) Compact Dissolution; (b) Conical Wormhole; (c) Dominant Wormhole; (d) Ramified Wormhole.

differences to the different solution methods and resolution. In the next chapter, we will perform the resolution study to address the second issue.

The variation in the type of wormhole formation with increasing velocity was obtained in Cohen's study as shown in the Fig. 4.3. The shape of the wormholes for a given velocity range is consistent with the experimental findings [1] and the later simulation studies [39]. Notice that a Darcy-type model was used in [2].

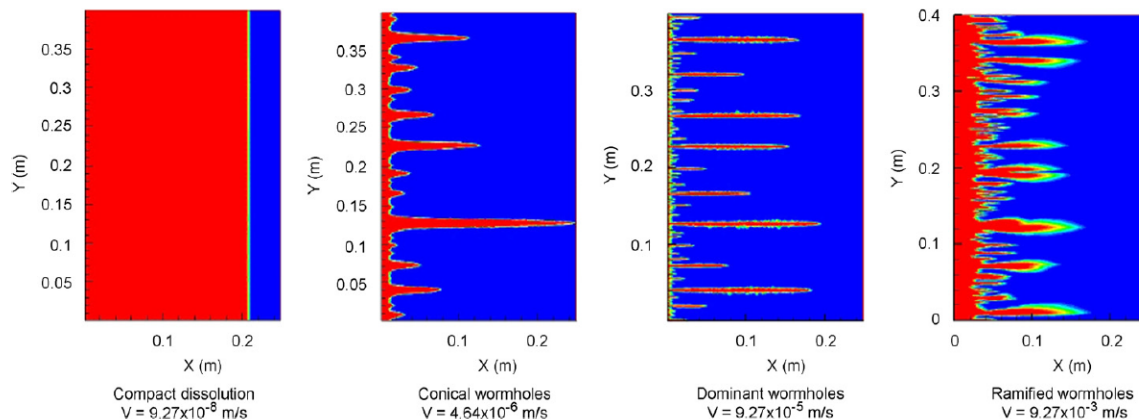


Figure 4.3: Wormhole dissolution patterns for increasing injection velocity. The red field represents region with 100% porosity. The resolution is 200 x 800 cells. Reprinted from [2].

4.3. Comparison with DBS model

In addition, we perform the comparison between results of simulation with Darcy and DBS model. Here we employed a newly introduced implementation of a separate momentum equation in AD-GPRS framework. In this implementation, the velocity at gridblock interfaces is used as independent variables.

The Darcy-Brinkman-Stokes model gave a result in agreement with the Darcy results as can be seen in Fig. 4.4. However, you can notice that the development of fingers and breakthrough moment happened much later with DBS approach than in the Darcy model as evident from the Fig. 4.4. The volume of the dissolved rock (red colour) in the DBS simulation after the injection of 0.7 PVI is not the same as the one in Fig. 4.3. This difference can be explained by the effect of the free flow which is only addressed in DBS model.

The results obtained by AD-GPRS are therefore consistent with the findings of Cohen et al. The differences in the source point of different wormholes in each domain is due to the difference in the degree of heterogeneity and the local permeability patches nearest to the injection face. Another key parameter that affects the quality of the results is numerical diffusion which will be discussed later. In addition, the DBS model seems to have a big impact on the results of wormhole propagation.

4.4. Comparison with 1D results

In this section, we compare the 2D results of simulation against the 1D results developed in Chapter 3. Here we study a cross-section of a 2D simulation. Since an exact comparison of 1D and 2D results is not expected to give any match, we, therefore perform a qualitative validation. For the current case, the dominant wormhole for a Darcy model is presented for several fractions of breakthrough time as illustrated

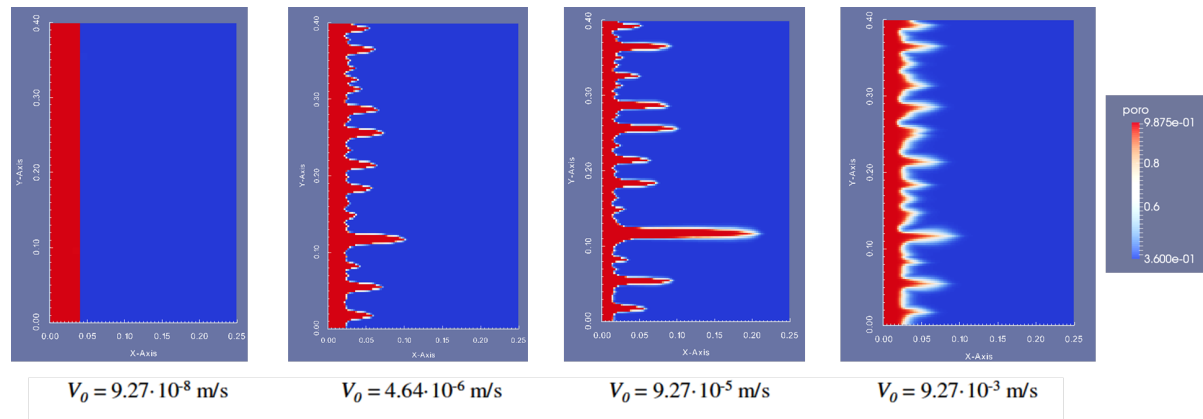


Figure 4.4: DBS model simulations with AD-GPRS. Wormhole dissolution patterns for increasing injection velocity: (a) Compact Dissolution; (b) Conical Wormhole; (c) Dominant Wormhole; (d) Ramified Wormhole.

in the Fig. 4.5. The most dominant wormhole is studied in this case, which is marked out in the figure.

The 1D results obtained from the cross section of 2D simulation are shown in the figure below. The porosity fields have the same shape and trend as obtained in Chapter 3. The pressure maps are a bit smeared and have a front that is leading with time. This can be addressed due to the variable velocity in x-direction, performed in the case of 2D simulation, as well as a limited (but still non-zero) flux in y-direction. These results confirm the fact that the wormhole propagation cannot be studied effectively by modelling of 1D wormhole propagation in idealistic assumptions.

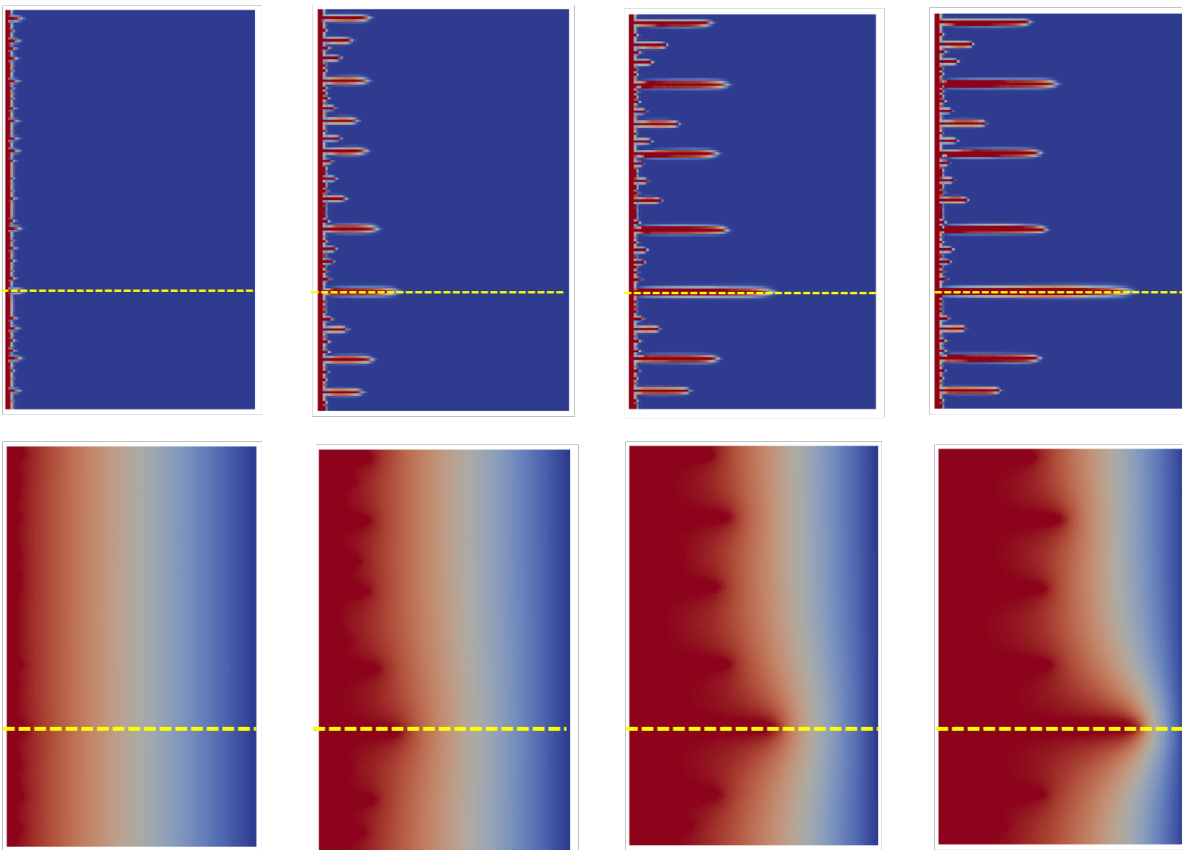


Figure 4.5: Darcy model - Dominant Wormhole dissolution patterns for increasing time.
Top : Porosity profiles ; *Bottom*: Pressure profiles for the times $T = 0.25T_{BT}$, $T = 0.5T_{BT}$, $T = 0.75T_{BT}$ and $T = 0.9T_{BT}$.

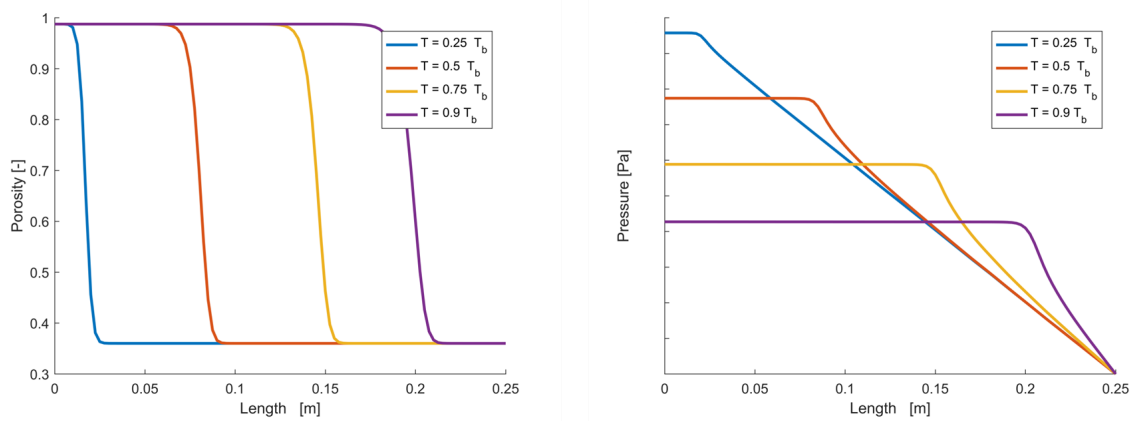


Figure 4.6: 1D results obtained from the cross-section marked in 4.5.
Left: Porosity profiles; *Right*: Pressure profiles for the times $T = 0.25T_{BT}$, $T = 0.5T_{BT}$, $T = 0.75T_{BT}$ and $T = 0.9T_{BT}$.

5

NUMERICAL CONVERGENCE STUDY

In this chapter, we will demonstrate that our solution is fully numerically converged independent of the type of wormhole formation for two models for momentum equation: Darcy and Darcy-Brinkman-Stokes. In addition, we will introduce the new characteristic – Pore Volumes for Breakthrough (**PVBT**) – to quantify the differences in solution independent from the wormhole pattern.

5.1. Effect of resolution on capturing the phenomenon

The impact of resolution is studied by simulating the acidisation on four degrees of resolution which are subjectively classified as follows: In Fig. 5.1 and Fig. 5.2 you

Very coarse	- [25x40] cells
Coarse	- [50x80] cells
Fine	- [100x160] cells
Very Fine	- [200x320] cells

can see the porosity distribution after injecting of 0.7 PVI at different resolutions for a conical wormhole regime. Although the finest scale used here has just 64,000 cells in comparison to 160,000 cells used by Cohen et al. [2], you can see that this resolution is sufficient to get fully convergent results. Here, to reduce the influence of heterogeneity of permeability to the convergence study, the heterogeneity pattern was generated for the coarsest model and downscaled to its finer resolutions.

Another trend evident from the figures of a wormhole in ramified regimes shown in Fig. 5.1 and Fig. 5.2. In all of these regimes, both the Darcy and DBS models give a faster breakthrough on finer-scale grid. This deviation of the results from the reference solution can be attributed to the effect of the numerical diffusion.

Every mathematical solution to a physical problem is usually an approximation with an error which depends on the numerical method adopted. In the case of solving the Advection-Diffusion equation, the first order of discretisation in space and time adds an additional 'spreading of the solution'. This smearing of the solution leads to the additional diffusive term and therefore the wormholes obtained are wider and propagate slower than the reference solution.

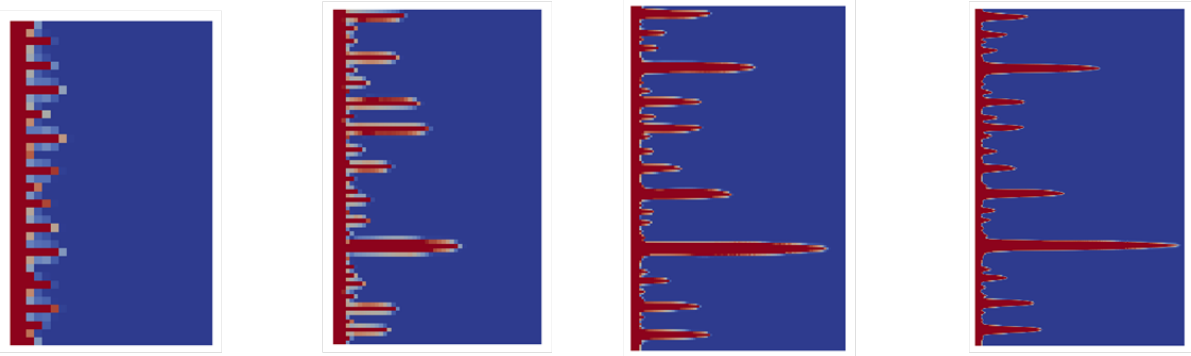


Figure 5.1: Darcy model - Conical wormhole at same 0.55 PVI for (a) Very Coarse [25×40], (b) Coarse [50×80], (c) Fine [100×160], (d) Very Fine [200×320] ($Q = 1.6 \cdot 10^{-4} m^3/day$).

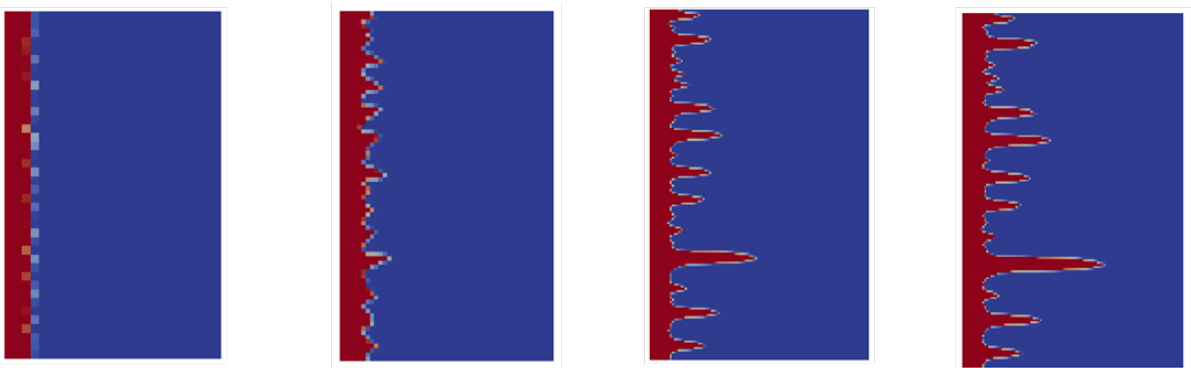
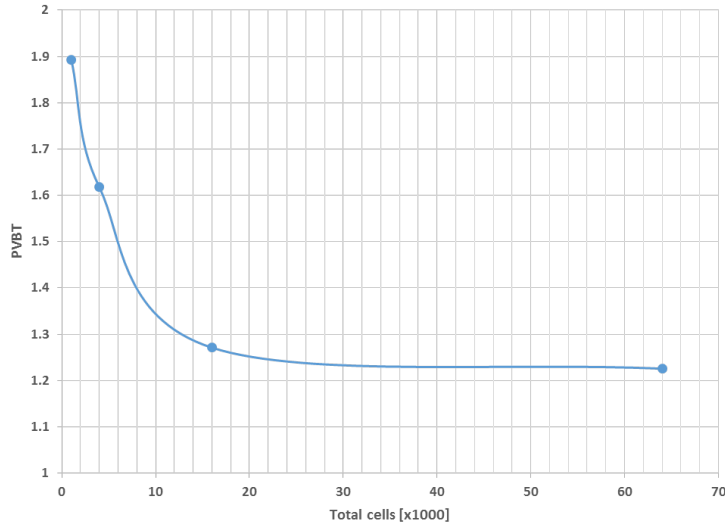


Figure 5.2: DBS model - Conical wormhole at same 0.55 PVI for (a) Very Coarse [25×40], (b) Coarse [50×80], (c) Fine [100×160], (d) Very Fine [200×320] ($Q = 1.6 \cdot 10^{-4} m^3/day$).

	[25x40]	[50x80]	[100x160]	[200x320]
Numerical Diffusion $[\frac{m^2}{day}]$	0.0432	0.0232	0.0132	0.008
Physical Diffusion $[\frac{m^2}{day}]$	8.6×10^{-5}	8.6×10^{-5}	8.6×10^{-5}	8.6×10^{-5}

Table 5.1: Comparison of numerical and physical diffusion coefficients.

For the employed numerical scheme, the mathematical form of numerical diffusion is $D_{Num} = \frac{1}{2} [\Delta x V + \Delta t \vec{V}^2]$, where Δx is the characteristic grid size, Δt is the characteristic timestep and \vec{V} is the characteristic velocity [40]. It can be mitigated by either reducing the grid-size or by cutting down the time-step for a given flow field. The apparent diffusion coefficient can be obtained by adding the physical diffusion coefficient and the numerical diffusion coefficient. Table 5.1 shows the reduction of D_{Num} with increasing resolution. As you can see in the first example of conical wormholes, even though the numerical diffusion is dominating against the physical diffusion at our finest resolution, the convergence of numerical results is already obtained at a resolution [100x160], which can be clearly seen from Fig. 5.3.

Figure 5.3: PV_{BT} decline with the increasing number of grid cells obtained for simulations in ADGPRS for ramified wormhole. DBS model was employed.

5.2. Pore Volumes for Breakthrough (PVBT) analysis

To quantify the convergence of the solution, we introduce the Pore Volumes for Breakthrough (PVBT) characteristics. This term corresponds to the volume of injected acid, measured in pore volumes, which is required for wormhole at particular regime to breakthrough. Using this characteristic, we can better quantify the convergence of the numerical solution. We start at low velocity regime where no wormholes observed at the front (see the first image in Fig. 5.4), which is the *compact dissolution* regime. Next, we enter the *conical wormhole* regime by increasing the injection velocity. In the conical regime, there is a single prominent or leading wormhole that channels most of the incoming flux. That explains much lower PVBT than in the compact regime.

With the increasing velocity, the wormholes start thinning due to more dominant dissolution in the tip of wormholes. This regime is the closest to our 1D simulation, where dissolution was only assumed in the tip of the wormhole. In addition, this is the most effective regime for both Darcy and DBS models as can be seen in Fig. 5.4. On further increasing the velocity, we can observe more wormholes, carrying the influx and dissolving more rock along it. Once in the *dominant regime*, there are multiple wormholes without a clear leading wormhole. This slows the breakthrough as illustrated in the Fig. 5.4. Moving into the *ramified regime*, there are multiple wormholes but the wormhole tips are now smeared and the penetration into the core is much weaker and hence the PVBT increases. The porosity fields corresponding to the points used in Fig. 5.4 and Fig. 5.5 are shown in Fig. 5.6.

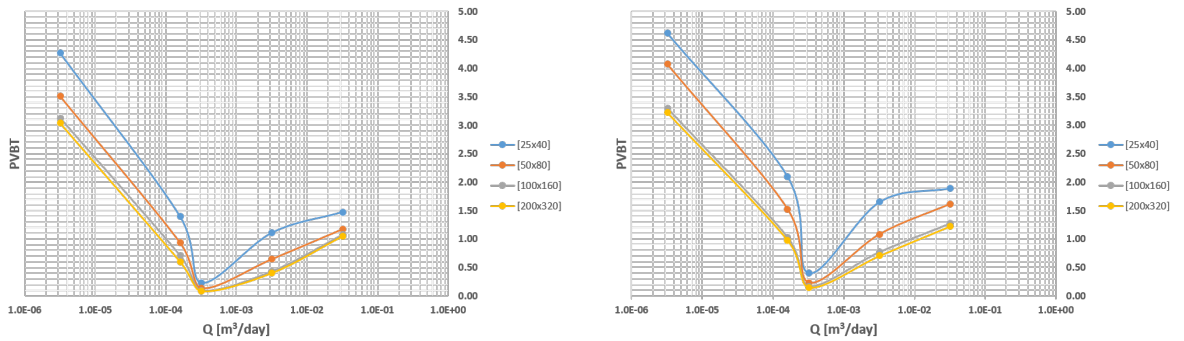


Figure 5.4: PVBT analysis for different resolutions. Left: Darcy model, Right: DBS model.

Taking a closer look at the Fig. 5.5, we can establish that the Darcy model always needs fewer pore volumes for breakthrough than the DBS model. This could be understood by the fact that in the Darcy model, we ignore the dissipative viscous forces term i.e $-\mu'\Delta\vec{V}$ term in every applicable grid cell. Whereas the DBS model takes these losses into account for the applicable cells (cells with both solid and fluid phases), hence the PVBT from this model is higher, in agreement with the accurate physics. A detail PVBT comparison with resolution can be found in section A.2 of the appendix.

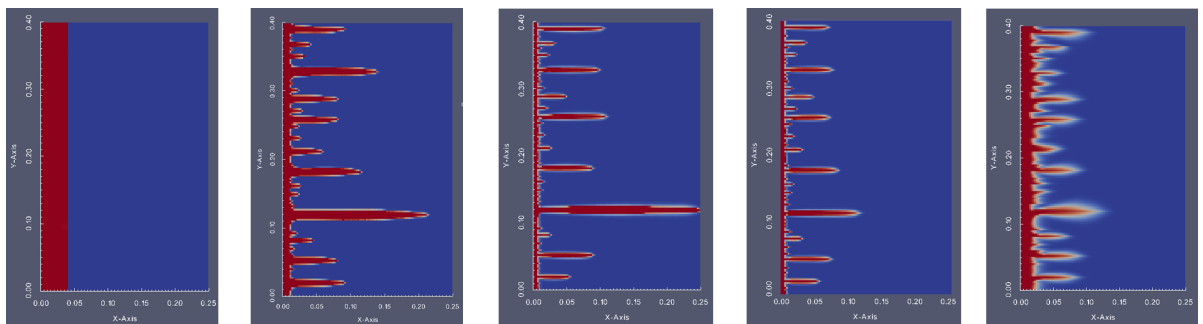


Figure 5.6: Porosity maps for the evolution of wormholes for changing velocity - Darcy model.

The breakthrough time is lower for a higher resolution due to the factors previously discussed. Fig. 5.5 shows the differences in the PVBT for Darcy and DBS models for a resolution of [100×160]. It is clear that the results converge at a resolution of [100×160] gridcells or higher resolution. The alternative error between the

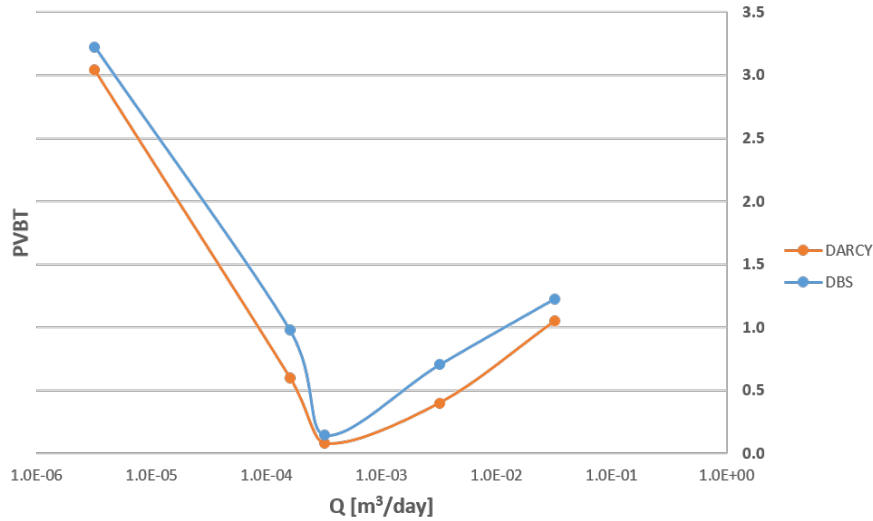


Figure 5.5: PVBT analysis comparison of Darcy and DBS for a resolution of [100x160].

[100×160] and [200×320] (discussed in appendix A.1) vanishes which is why the results presented in the further chapters were performed for the convergent resolution of [100×160].

5.3. Convergence of the wormhole length

The metric, presented in the previous section, corresponds to the breakthrough time may not be sufficient to measure the convergence of solution. That is why we decided to check another metric suggested by in the experimental works of McDuff et al. [41] This metric represent the ratio of the length of the leading wormhole to the length of the average wormhole which we call γ ratio. The γ ratio has a maximum in between

before the dominant regime and decreases on either side of this regime as can be seen in Fig. 5.7. For a low-velocity injection (compact regime) this parameters is $\gamma = 1$ as there is no wormholes. Similarly, for the high-velocity injection i.e. for ramified dissolution, there are no distinct leading wormholes and the γ ratio again close to 1 as depicted in the figure 5.7. It is interesting that in this regime, the maximum is reached at the dominant regime and not corresponds to the optimal regime in terms of breakthrough (which is between the dominant and conical regimes). The average wormhole length is measured for a near breakthrough of the 25 cm x 40 cm heterogeneous block previously discussed in chapter 3. The image analysis to obtain and count the length of wormhole was done in the public image analysis software Fiji [42] with simple binary operations.

The Fig. 5.8 demonstrates the difference in the mesh convergence analysis of the two models. The comparisons for other resolutions can be found in Fig. A.3 in the appendix. The γ ratio plot almost overlaps for the finest resolution in our study. We can therefore conclude from Fig. 5.7 that the solution converges and becomes independent of the grid resolution for model with [100×160] cells and higher. This conclusion is valid for both Darcy and DBS models.

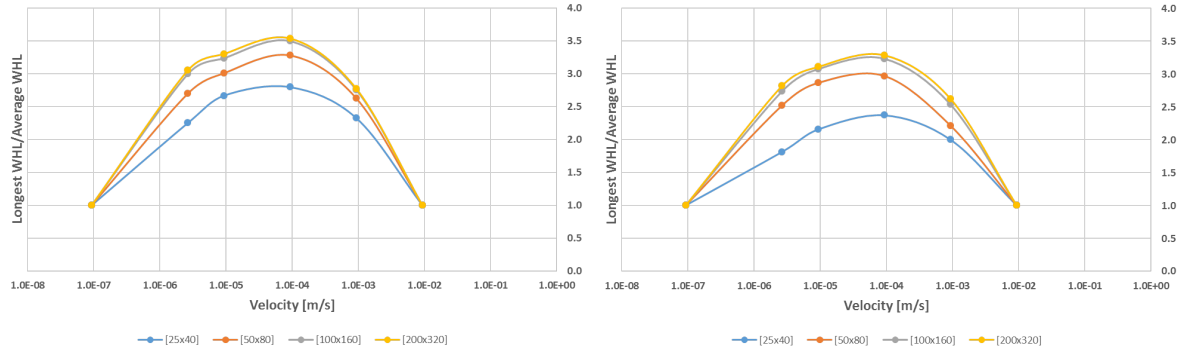


Figure 5.7: Ratio of length of the leading wormhole to the length of the average wormhole for (a) Darcy model (b) DBS model.

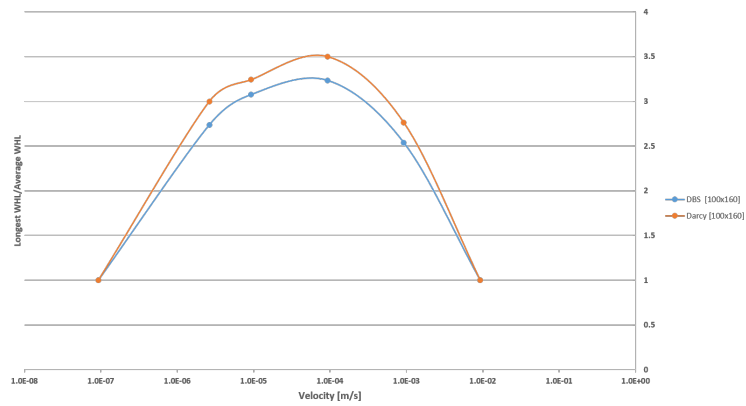


Figure 5.8: Comparison of ratio of length of the leading wormhole to the length of the average wormhole for Darcy and DBS models for a resolution of [100x160].

5.4. Nonlinear performance analysis

To test the nonlinear performance of simulation with Darcy and DBS models, two sets of simulations were run on the convergent fine scale for each of the models. Parallel Sparse Direct Solver (PARDISO) [27] is used to solve the linear system. The system was run at TU Delft cluster node with 4 threads on Intel Xenon CPU E5-2650 with clock rate of 2.3 GHz. The comparison of the timesteps and non-linear iterations of two models are shown in Fig. 5.9 and Fig. 5.10.

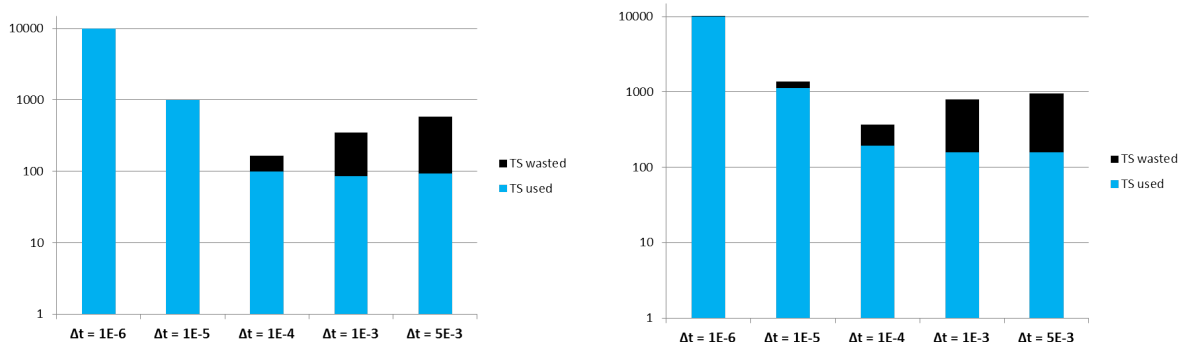


Figure 5.9: Time steps statistics comparison for a simulation time of 0.01 days for different timesteps. *Left* : Darcy model ; *Right* : DBS model

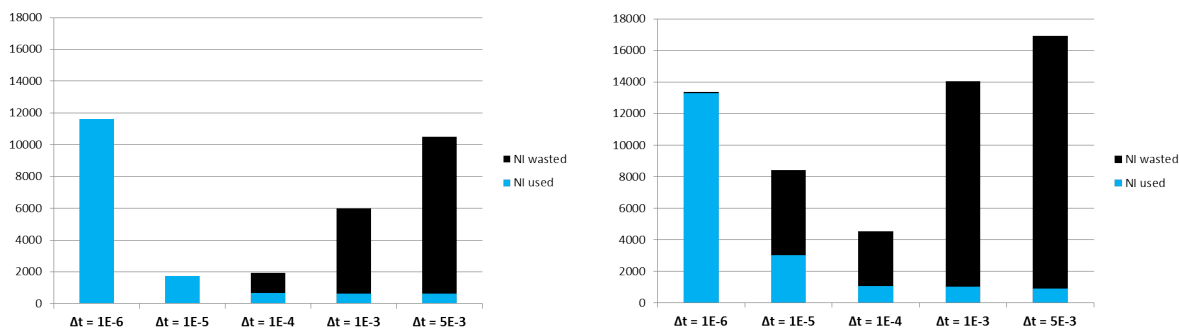


Figure 5.10: Newton Iterations statistics comparison for a simulation time of 0.01 days for different timesteps. *Left* : Darcy model ; *Right* : DBS model

The results clearly show that the DBS model requires more timesteps to converge in comparison to Darcy model. The sensitivity to timesteps is also quite different for both models (notice that y-axis of Fig. 5.9 is in log-scale). It is also clear that both models have a particular limit in timestep size when non-linear solver is able to converge without wasting iterations. This requires a development of a better non-linear solver for this type of simulations.

5.5. Conclusive remarks

In this chapter, we found through the PVBT analysis that the Darcy model requires fewer pore volumes for breakthrough in comparison to the DBS model. The difference in these two solutions comes with the additional treatment of dissipative viscous forces in the DBS solution. We also introduced the numerical diffusion and found it to be dominating the physical diffusion. This could be tackled by modelling for an extremely fine scale, as shown in [2], which quickly becomes computationally expensive. Our convergence analysis exhibit the fact that a resolution of $[100 \times 160]$ is

reasonably sufficient for the non-linear convergence presented in terms of the breakthrough pore volume and wormhole length. Finally, the non-linear performance analysis revealed a need for a better non-linear solver to perform simulation at larger timesteps.

6

SENSITIVITY STUDY

Next, we will perform a sensitivity study of the simulation results to various parameters. Numerically convergent results are chosen and the effect of dimensionless numbers, heterogeneity, geometry and flow parameters is investigated. A benchmark performance analysis of the two methods is also presented. Finally, the effect of a second (gas) phase on the wormhole breakthrough is also investigated.

6.1. Representation in dimensionless numbers

Any physical phenomenon can be characterised by a limited number of parameters called dimensionless numbers. In order to better quantify and characterise the wormhole formation, we rely on two important dimensionless numbers – Peclet (**Pe**) and Damkohler (**Da**) numbers. These numbers can be used to compare different wormhole models and to determine optimum operation regime in terms of these dimensionless numbers.

The Damkohler number is defined as the ratio of reaction rate to advection rate. It gives an insight into controlling the shape of the wormhole. For instance, if the reaction rate is much larger than advection rate, the acid, flowing through the carbonate rock, dissolves it rapidly, thereby leading to a compact dissolution face (leftmost point in Fig. 6.1). If the reaction rate is balanced with the advection rate, an ideal operating range can be obtained i.e in the dominant wormhole regime as evident from the figure where the PVBT is minimum.

The Damkohler number is given by

$$Da = \frac{l\alpha}{V_o}$$

In the case of optimising the wormhole formation and growth, the following things can help us to improve the engineering of the acid job - higher permeability, sufficiently high diffusion so that the wormholes are wide enough while penetrating the rock and a higher velocity to aid it. All these three factors can be quantified as the ratio of mass transport due to convection and transport due to diffusion, which corresponds to the dimensionless number called Peclet number.

The Peclet number is given by

$$Pe = \frac{lV_o}{D}$$

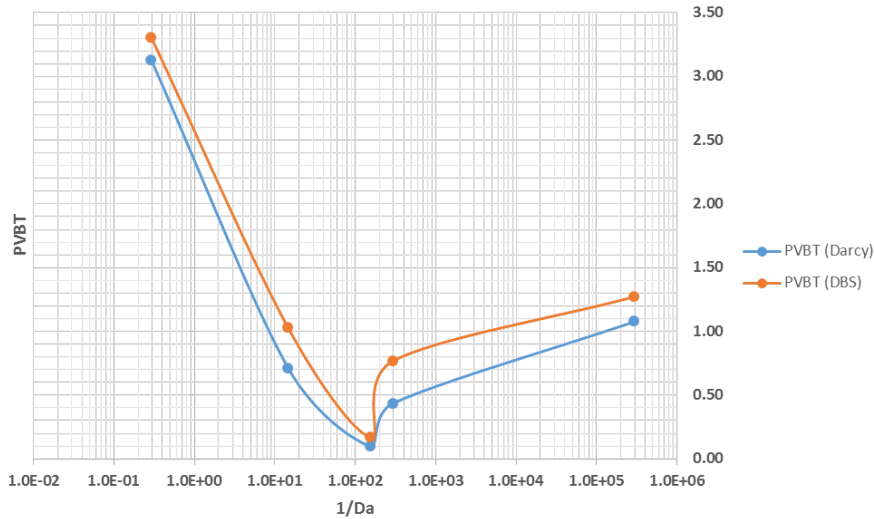


Figure 6.1: Analysis of PVBT with changing Damkohler number

In agreement with the optimisation plot obtained for Damkohler number, we observe a similar shape for Peclet number. At intermediate Peclet number, the wormhole is growing fast enough and is wide enough which leads to lowest PVBT as illustrated in 6.2.

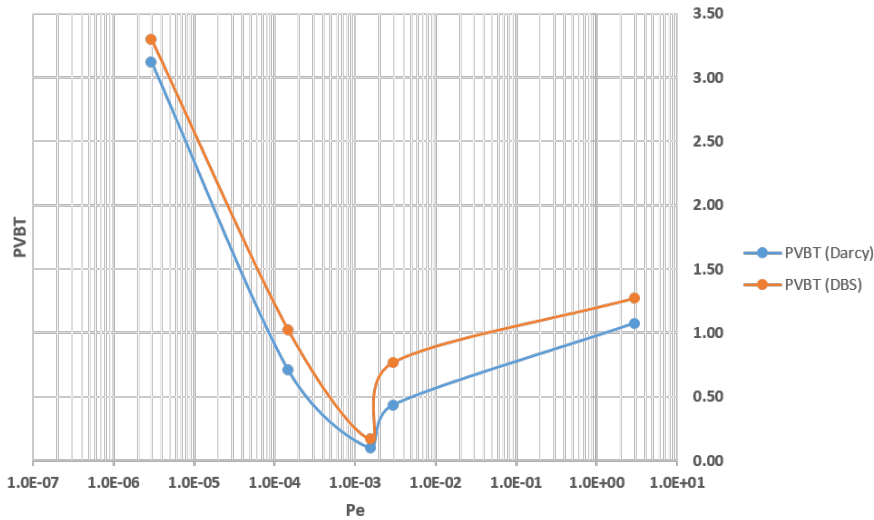


Figure 6.2: Analysis of PVBT with changing Peclet number

6.2. Effect of confinement on wormhole formation

In this section, we look into the effect of the confinement to the performance of the acidisation process. Most of the publications, cited in our study deal with "confined" conditions, i.e. the situation where the wormhole length is longer than the injection face. To demonstrate the effect of this confinement or the geometry effect on the wormhole growth, three aspect ratios are considered, with a fixed width of 0.25 m and variable heights of 0.4 m, 0.1 m and 0.05 m. The first ratio can be considered as

unconfined when two others are *confined*. The results of simulations for the conical regime of injection is shown in Fig. 6.3.

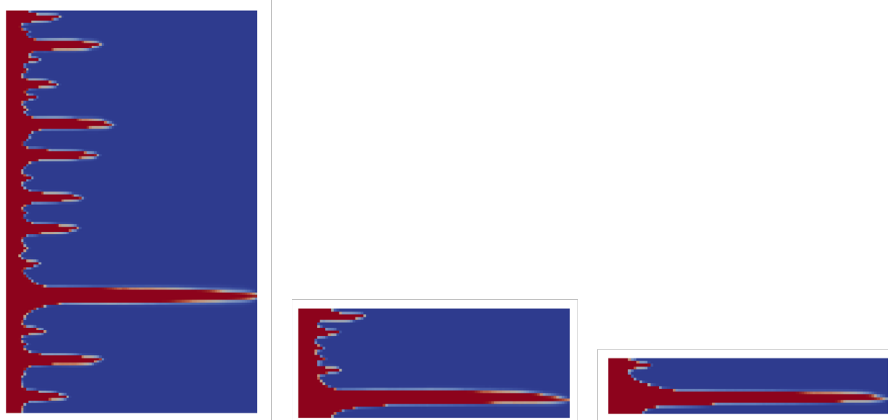


Figure 6.3: DBS model - Wormholes formation in (a) unconfined condition with a height of 0.4 m (b) confined conditions with height of 0.1 m (c) confined with 0.05 m height

It can be noticed that in Fig. 6.3 (b) and (c), there is only one leading wormhole that has formed. This phenomenon can be explained in terms of influx distribution and competition. In the first case, there is a lot of contention between the wormholes but also a lot of space between the primary and secondary wormholes. This enables the flux to be distributed to the secondary wormholes, although sparsely. But, in the case of the other two scenarios, there is not much spacing between the wormholes and hence all the flux goes into the dominating wormhole with a very limited formation of the secondary wormholes.

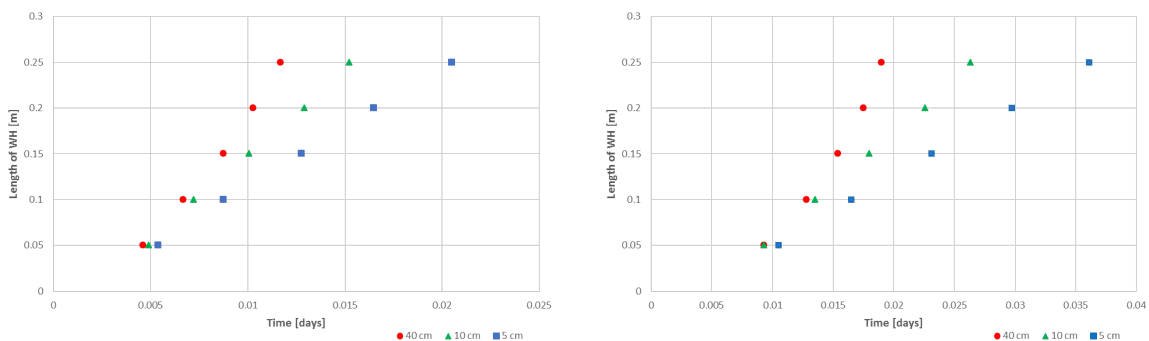


Figure 6.4: Wormhole growth in the Darcy (left) and DBS (right) models for different confinement ratios.

The wormhole dynamics for Darcy and DBS models are presented in the Fig. 6.4. Here we plot the length of dominating wormhole vs. time. Notice, that in the confined models, the wormhole growth is almost linear while for an unconfined model, it deviates from the linear behaviour due to interactions with secondary wormholes. That may affect the perception of the optimal dissolution regimes obtained from simulation studies.

6.3. Effect of heterogeneity

The effect of heterogeneity on the wormhole dynamics has a controversial interpretation in the published studies. In this thesis, we will try to limit the study to two

factors - the growth of the most dominant wormhole with time and the number of dominant wormholes vs. the heterogeneity amplitude.

Keeping the same parameters, we increase the heterogeneity amplitude of permeability for a dominant regime. We used permeability perturbations ΔK of 5%, 10% and 20%. The porosity distributions for all three amplitudes in the case of Darcy and DBS models are shown in Fig. 6.5 and Fig. 6.6 respectively. Based on these results, there is a limited sensitivity of the wormhole distribution to the heterogeneity amplitude.

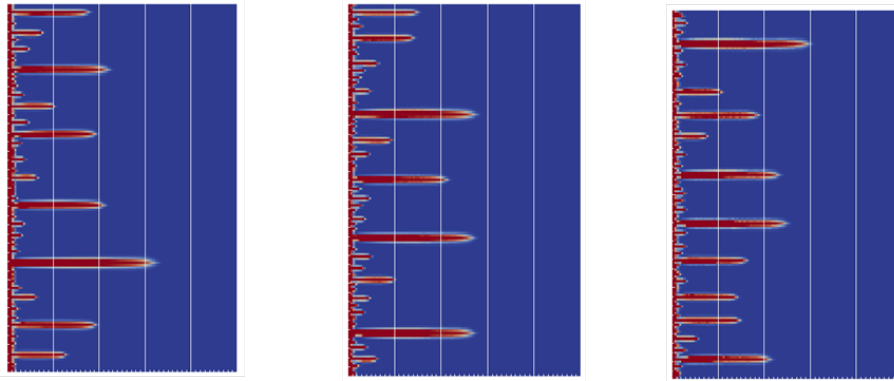


Figure 6.5: Porosity maps for Darcy model for permeability perturbation of 5% 10% and 20% showing several dominant wormholes.

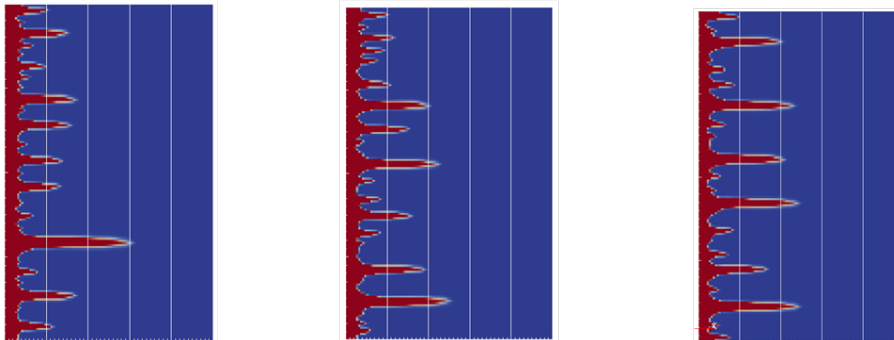


Figure 6.6: Porosity maps for DBS model for permeability perturbation of 5% 10% and 20%.

However, this conclusion is changing if we look into the sensitivity of dominant wormhole length as function of time. From Fig. 6.7 it is clear that for $\Delta K = 20\%$ the length of the leading wormhole lags behind for cases with lower amplitude. This behaviour can be understood by taking a closer look the porosity maps in Fig. 6.7. As the heterogeneity amplitude increases, the number of wormholes increases which leads to less competition between the wormholes. As a result, the breakthrough time is changing proportional to the heterogeneity amplitude.

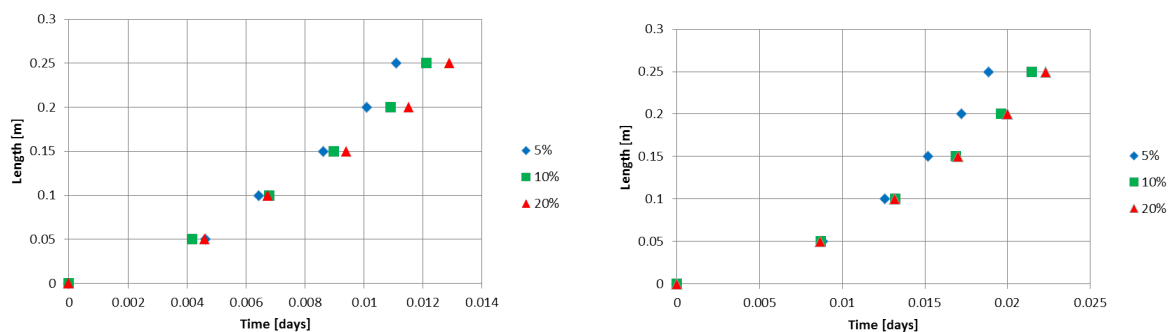


Figure 6.7: Wormholing dynamics for Darcy (left) and DBS (right) models for permeability perturbation of 5% 10% and 20%.

6.4. Two phase modelling of acidisation : CO₂ co-injection

CO₂ capture and storage (CSS) is one of the most promising and emerging atmospheric CO₂ emission reduction technologies [43, 44]. Amongst the CSS methods, the sequestration in deep sedimentary reservoirs is the most attractive due to the large storage capacity, relatively low cost, and minimal environmental impact [45]. This geological storage of CO₂ can either be performed by physical trapping or by solubility trapping, amongst other strategies [46, 47]. For the former, the CO₂ is dissolved into the brine and form carbonic acid, which is then co-injected with CO₂ in gaseous phase.

Unlike the well stimulation projects for oil recovery, the wormhole patterns in such CO₂ co-injection are more complicated due to the presence of the second phase. The single phase acidisation is governed and optimised with dimensionless numbers such as Peclet and Damkohler numbers by changing the flow rate, acid type, permeability field as discussed in the previous sections. While the single phase acidising with an acid (liquid phase) injection occurs through matrix dissolution, it becomes quite different with CO₂ co-injection. The CO₂ first dissolves in the fluid phase and forms carbonic acid (H₂CO₃) which in turn dissolves the matrix. This delayed dissolution leads to a deeper penetration and hence a better acid job as a consequence. Therefore, a co-injection of CO₂ and acid such as HCl could yield a better and quicker breakthrough result in case carbonic acid can be formed.

In the present study, we simulate the effect of CO₂ co-injection along with an immiscible acid component. The net volumetric injection rate of the acid is kept the same as previous experiments while the net CO₂ mole fraction is now increased from 0 to 0.1. In our simulations, we ignored the formation of carbonic acid. That is why not much of a difference is observed in the pore volume needed for breakthrough in both Darcy and DBS models, which is evident from figures 6.8 and 6.9.

The PVBT plots obtained for two-phase co-injection reveal a slight increase in pore volumes needed for breakthrough, consistent with the experimental studies by Ott and Oedai [48]. A closer look must be taken at the CO₂ concentration and its localisation in order to understand the reason for the delayed breakthrough. Also, the DBS model, used here, does not include an accurate treatment of two phase flow in momentum equations and can only be seen as an idealistic approximation.

The physical phenomenon for the inhibition of the wormholes can be understood by observing figure 6.10. As the wormholes are formed by the reactive liquid phase, the CO₂ in the gas phase rushes into the dissolved wormhole channels. Also, since

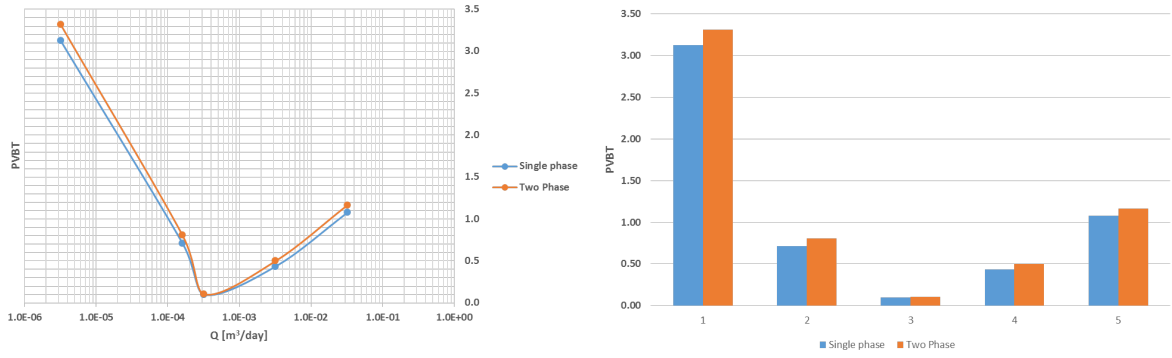


Figure 6.8: PVBT analysis of two phase and comparison with single phase with Darcy model.

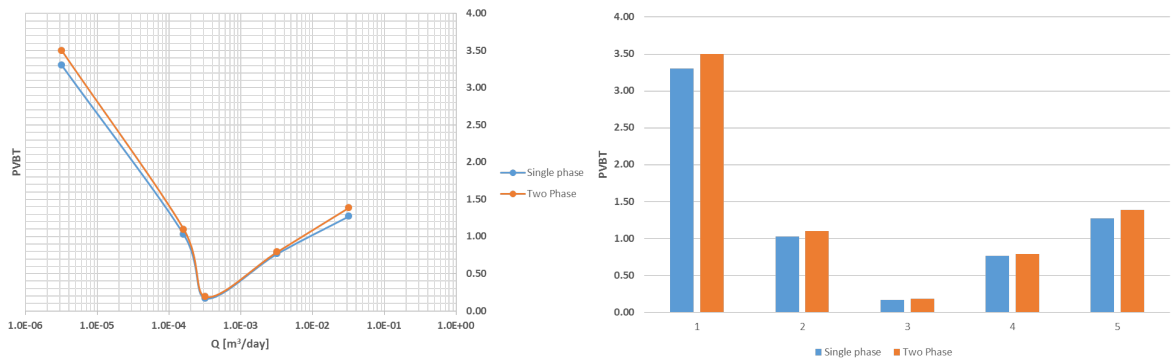


Figure 6.9: PVBT analysis of two phase and comparison with single phase with DBS model.

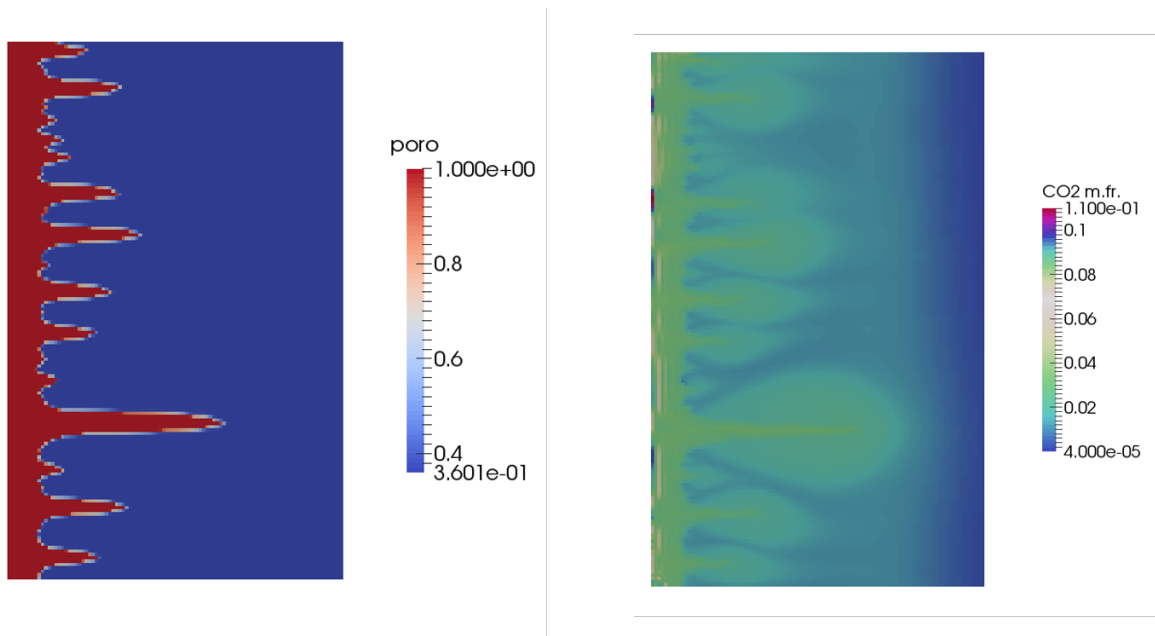


Figure 6.10: Smearing and retardation of wormholes due to CO_2 co-injection. a) Porosity field of conical wormhole b) CO_2 concentration around wormhole.

CO₂ has a higher mobility than the liquid phase, it diffuses into the porous media around the wormholes. Since CO₂ is not reactive in this case, it prevents the reactive acid from penetrating further into the porous matrix, thereby leading to a net inhibition and accounting to a higher PVBT than in the single phase case. This is consistent with the experimental and simulation studies performed by Izgec et al. [49] in which the retardation of the wormhole growth was recorded in the CT scan.

7

CONCLUSIONS AND FUTURE WORK

In this research, the problem of acidisation was studied using two different modelling approaches. The first is the conventional Darcy scale modelling using the volume based averaging of Darcy's law. The second modelling approach involved a single domain micro-continuum approach i.e. the hybrid modelling with the Darcy-Brinkman-Stokes modelling. Hybrid modelling is valid for regions where Darcy's law fails and it also removes the complexity of dealing with jumps in properties at the interface as these changes get translated in terms of effective coefficients like porosity and permeability. The hybrid model works in porous media, open channels and in the transition region.

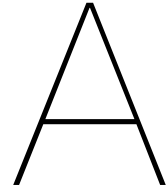
The first model was implemented in MATLAB and corresponds to an idealistic propagation of a single wormhole in Darcy assumptions. The 2D modelling was performed using Stanford University's Automatic Differentiation General Purpose Research Simulator (ADGPRS). Here, both Darcy and Darcy-Brinkman-Stokes (DBS) models were used for the momentum equation. In 2D, distinct differences were observed in terms of the wormhole shapes in Darcy and DBS models. In terms of Pore Volume for Breakthrough (PVBT), the Darcy model gave consistently lower PVBT than the DBS model. Physically, it can be attributed to the discounting of dissipative viscous forces in the Darcy model.

A further analysis on the resolution indicates a dependency of numerical results. A mesh convergence analysis confirmed the minimum grid resolution to capture the phenomenon accurately. Translation of the results into dimensionless numbers gave us an optimal regime in terms of Damkohler and Peclet numbers, though there is a debate on the definitions of optimal conditions and several researchers deviated from these conventional dimensionless numbers to formulate other variables and report the best operating conditions.

The effect of geometry on the development of wormholes, i.e on wormhole dynamics, was investigated as well. It was found that under unconfined conditions, there is strong wormhole competition and therefore the PVBT is lower. Another factor affecting the wormhole propagation is the amplitude of the rock heterogeneity. A larger perturbation influenced the number of wormholes formed and thereby affecting the breakthrough time. An analysis of the nonlinear convergence revealed a need for a better nonlinear solver to perform more effective computations. Finally, the influence of co-injected CO₂ in simplified assumptions was found to play a negative effect as it retarded wormhole growth dynamics.

For the future research, the following broader frameworks can be considered:

- A more accurate chemical description of the system can be employed by taking into account a real chemical reactions with multiple species.
- The effect of thermodynamics on the chemical kinetic model and phase equilibrium can be investigated with the implementation of a thermodynamic model.
- Studies have revealed a difference in the 2D and 3D models [2, 39]. The difference in Darcy and DBS model can be studied for a 3D model, where true fractal shapes in wormholes can be observed.
- A detailed multiphase model should be developed with the presence of gas and oil phase.
- An experimental study is required to further validate the simulation results.



APPENDIX

A.1. Convergence study with resolution : Relative Error

The convergence of the solution, as discussed in chapter 5 was found for a resolution of [100×160] or finer resolution. Here we present the relative error with respect to the finest resolution i.e. for [200×320]. As Fig.A.1 illustrates, the relative error is high for coarser resolution and becomes minuscule for a resolution of [100×160] which justifies using this for performing sensitivity studies.

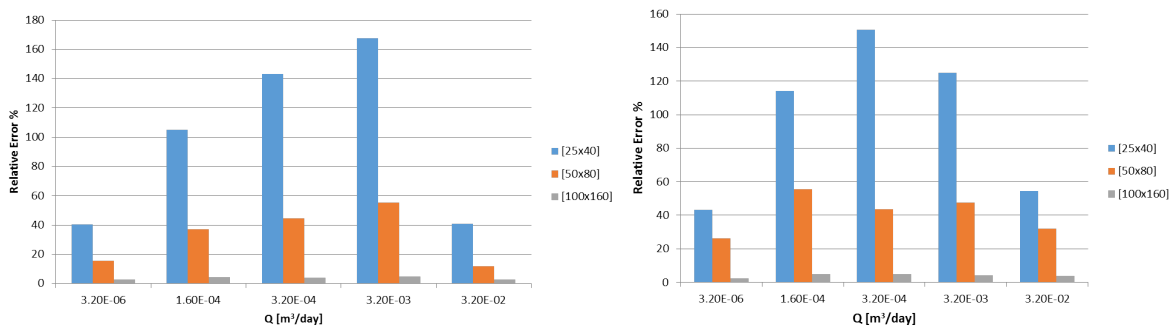


Figure A.1: Relative Error % in PVBT for (a) Darcy model (b) DBS model relative to the [200x320] solution.

A.2. Exhaustive comparison of Darcy and DBS results

Here, the comparison of the Darcy and DBS models is done for different resolution in Fig. A.2 which demonstrate convergence on increasing resolution. Note that the Darcy model always needs fewer pore volumes of fluid injected to breakthrough. Another way we check the convergence is by defining the ratio of length of the leading wormhole to the length of the average wormhole which is given in the Fig.A.3. This further affirms the convergence in resolution.

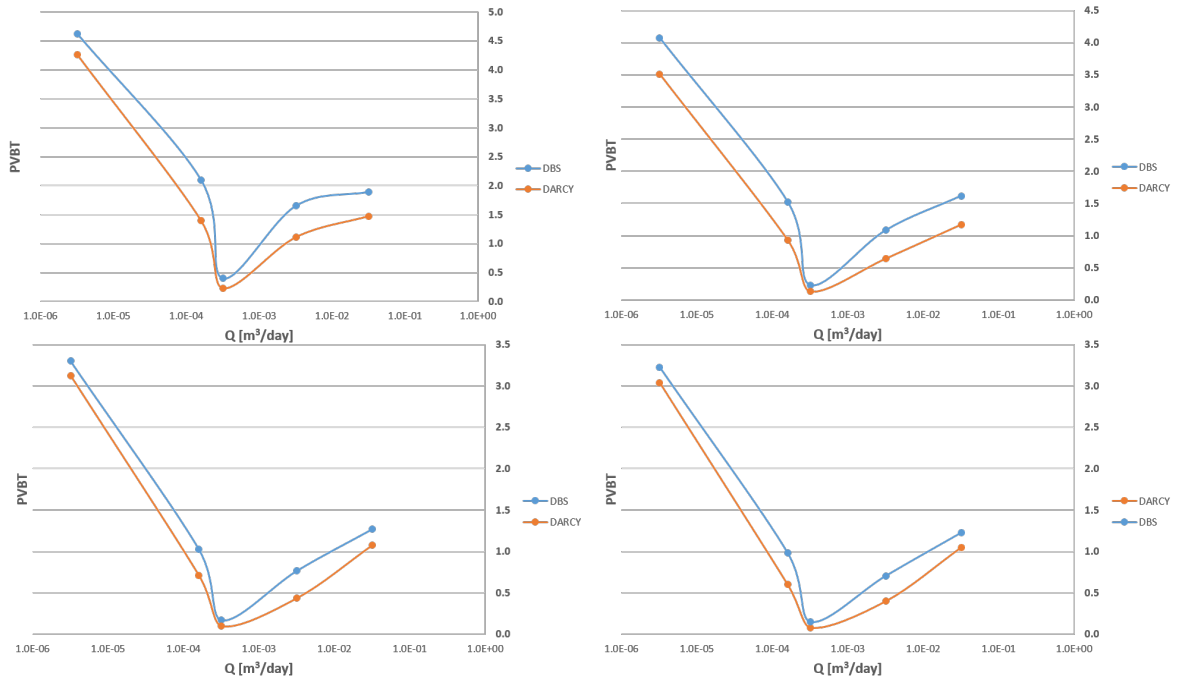


Figure A.2: PVBT analysis comparison of Darcy (left) and DBS (right) for a resolutions of top :[25x40] [50x80] , bottom : [100x160] [200x320]

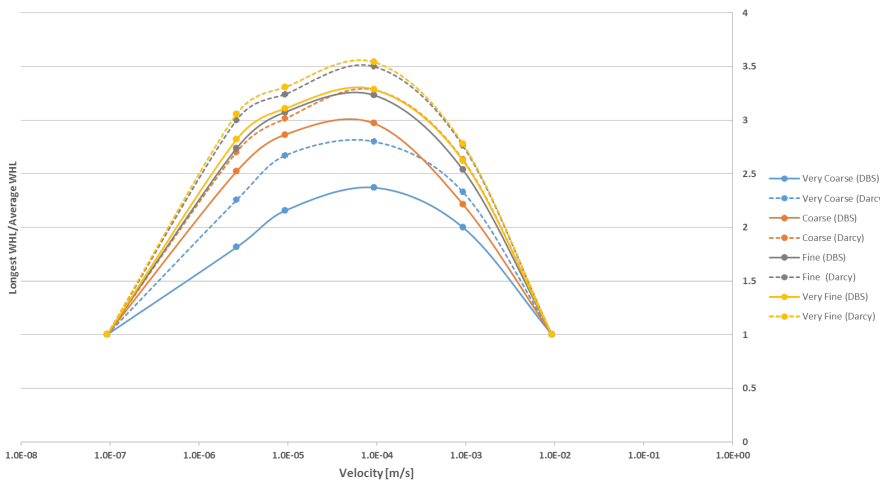


Figure A.3: Comparison of ratio of length of the leading wormhole to the length of the average wormhole for Darcy and DBS models.

Bibliography

- [1] F Golfier, C ZArcone, B Bazin, R Lenormand, D Lasseux, and M Quintard. On the ability of a darcy-scale model to capture wormhole formation during the dissolution of a porous medium. *Journal of fluid Mechanics*, 457:213–254, 2002.
- [2] Charles Edouard Cohen, Didier Ding, Michel Quintard, and Brigitte Bazin. From pore scale to wellbore scale: Impact of geometry on wormhole growth in carbonate acidization. *Chemical Engineering Science*, 63(12):3088–3099, 2008.
- [3] Curtis Crowe and Ron Thomas. Trends in matrix acidizing. *Oilfield Review series, Schlumberger*, 10, 1992.
- [4] Robert C Earlougher Jr. Advances in well test analysis, henry l. *Doherty series, Monograph*, 5, 1977.
- [5] L.A. Barrios, J.E. Quijano, R.E. Romero, H. Mayorga, M. Castro, and J. Caldera. Enhanced permeability by chemical stimulation at the berlin geothermal field, el salvador. pages 73–78, 2002.
- [6] J.G. Jaimes-Maldonado and R. Sánchez-Velasco. Acid stimulation of production wells in las tres vírgenes geothermal field, bcs, méxico. volume 27, pages 699–705, 2003.
- [7] George A Xydis, Evanthia A Nanaki, and Christopher J Koroneos. Low-enthalpy geothermal resources for electricity production: A demand-side management study for intelligent communities. *Energy policy*, 62:118–123, 2013.
- [8] Sandrine Portier, François-David Vuataz, Patrick Nami, Bernard Sanjuan, and André Gérard. Chemical stimulation techniques for geothermal wells: experiments on the three-well egs system at soultz-sous-forêts, france. *Geothermics*, 38(4):349–359, 2009.
- [9] Leonard Kalfayan. *Production enhancement with acid stimulation*. Pennwell Books, 2008.
- [10] Nitika Kalia and Vemuri Balakotaiah. Modeling and analysis of wormhole formation in reactive dissolution of carbonate rocks. *Chemical Engineering Science*, 62(4):919–928, 2007.
- [11] Henry Darcy. Les fontaines publique de la ville de dijon. *Dalmont, Paris*, 647, 1856.
- [12] Vivek Swami, Christopher R Clarkson, Antonin Settari, et al. Non-darcy flow in shale nanopores: do we have a final answer? In *SPE Canadian unconventional resources conference*. Society of Petroleum Engineers, 2012.
- [13] Cyprien Soullaine and Hamdi A Tchelepi. Micro-continuum approach for pore-scale simulation of subsurface processes. *Transport in Porous Media*, 113(3):431–456, 2016.

- [14] Cyprien Soullaine. On the origin of Darcy's law. 2015.
- [15] Mohan KR Panga, Murtaza Ziauddin, and Vemuri Balakotaiah. Two-scale continuum model for simulation of wormholes in carbonate acidization. *AIChE journal*, 51(12):3231–3248, 2005.
- [16] Pavel Tomin and Ivan Lunati. Hybrid multiscale finite volume method for two-phase flow in porous media. *Journal of Computational Physics*, 250:293–307, 2013.
- [17] Pavel Tomin and Ivan Lunati. Spatiotemporal adaptive multiphysics simulations of drainage-imbibition cycles. *Computational Geosciences*, 20(3):541–554, 2016.
- [18] Pavel Tomin and Ivan Lunati. Investigating darcy-scale assumptions by means of a multiphysics algorithm. *Advances in Water Resources*, 95:80–91, 2016.
- [19] HC Brinkman. A calculation of the viscous force exerted by a flowing fluid on a dense swarm of particles. *Applied Scientific Research*, 1(1):27–34, 1949.
- [20] Automatic Differentiation General Purpose Research Simulator (AD-GPRS). <https://supri-b.stanford.edu/research-areas/ad-gprs>.
- [21] Denis V. Voskov and Hamdi A. Tchelepi. Comparison of nonlinear formulations for two-phase multi-component EoS based simulation. *Journal of Petroleum Science and Engineering*, 82–83:101 – 111, 2012.
- [22] Denis Voskov. An extended natural variable formulation for compositional simulation based on tie-line parameterization. *Transport in porous media*, 92(3):541–557, 2012.
- [23] Sara F Farshidi, Yaqing Fan, Louis J Durlofsky, Hamdi A Tchelepi, et al. Chemical reaction modeling in a compositional reservoir-simulation framework. In *SPE Reservoir Simulation Symposium*. Society of Petroleum Engineers, 2013.
- [24] Ruslan Rin, Pavel Tomin, Timur Garipov, Denis Voskov, Hamdi Tchelepi, et al. General implicit coupling framework for multi-physics problems. In *SPE Reservoir Simulation Conference*. Society of Petroleum Engineers, 2017.
- [25] Ruslan Rin. *Implicit Coupling Framework for Multi-Physics Reservoir Simulation*. PhD thesis, STANFORD UNIVERSITY, 2017.
- [26] R. Fucinos, D. Voskov, and A. K. Burnham. Hierarchical coarsening of simulation model for in-situ upgrading process. In *Society of Petroleum Engineers - SPE Reservoir Simulation Conference*, 2017.
- [27] Olaf Schenk and Klaus Gärtner. Solving unsymmetric sparse systems of linear equations with pardiso. *Future Generation Computer Systems*, 20(3):475–487, 2004.
- [28] Kambiz Vafai. *Handbook of porous media*. Crc Press, 2015.
- [29] Donald A Nield and Adrian Bejan. *Convection in porous media*, volume 3. Springer, 2006.

- [30] J Alberto Ochoa-Tapia and Stephen Whitaker. Heat transfer at the boundary between a porous medium and a homogeneous fluid: the one-equation model. *Journal of Porous Media*, 1(1), 1998.
- [31] B Goyeau, D Lhuillier, D Gobin, and MG Velarde. Momentum transport at a fluid-porous interface. *International Journal of Heat and Mass Transfer*, 46(21):4071–4081, 2003.
- [32] P Bousquet-Melou, B Goyeau, Michel Quintard, F Fichot, and D Gobin. Average momentum equation for interdendritic flow in a solidifying columnar mushy zone. *International journal of heat and mass transfer*, 45(17):3651–3665, 2002.
- [33] CT Hsu and P Cheng. Thermal dispersion in a porous medium. *International Journal of Heat and Mass Transfer*, 33(8):1587–1597, 1990.
- [34] K Vafai and CL Tien. Boundary and inertia effects on flow and heat transfer in porous media. *International Journal of Heat and Mass Transfer*, 24(2):195–203, 1981.
- [35] Cyprien Soullaine, Filip Gjetvaj, Charlotte Garing, Sophie Roman, Anna Russian, Philippe Gouze, and Hamdi A Tchelepi. The impact of sub-resolution porosity of x-ray microtomography images on the permeability. *Transport in Porous Media*, 113(1):227–243, 2016.
- [36] Cyprien Soullaine, Sophie Roman, Anthony Kovscek, and Hamdi A Tchelepi. Mineral dissolution and wormholing from a pore-scale perspective. *Journal of Fluid Mechanics*, 827:457–483, 2017.
- [37] Josef Kozeny. Uber kapillare leitung der wasser in boden. *Royal Academy of Science, Vienna, Proc. Class I*, 136:271–306, 1927.
- [38] Philip Crosbie Carman. Fluid flow through granular beds. *Transactions-Institution of Chemical Engineeres*, 15:150–166, 1937.
- [39] P Maheshwari, RR Ratnakar, N Kalia, and V Balakotaiah. 3-d simulation and analysis of reactive dissolution and wormhole formation in carbonate rocks. *Chemical Engineering Science*, 90:258–274, 2013.
- [40] Khalid Aziz and Antonin Settari. *Petroleum reservoir simulation*. Chapman & Hall, 1979.
- [41] Darren McDuff, Chris E Shuchart, Shalawn Jackson, Dieter Postl, James Seay Brown, et al. Understanding wormholes in carbonates: Unprecedented experimental scale and 3-d visualization. In *SPE Annual Technical Conference and Exhibition*. Society of Petroleum Engineers, 2010.
- [42] Johannes Schindelin, Ignacio Arganda-Carreras, Erwin Frise, Verena Kaynig, Mark Longair, Tobias Pietzsch, Stephan Preibisch, Curtis Rueden, Stephan Saalfeld, Benjamin Schmid, et al. Fiji: an open-source platform for biological-image analysis. *Nature methods*, 9(7):676–682, 2012.
- [43] JCM Pires, FG Martins, MCM Alvim-Ferraz, and M Simões. Recent developments on carbon capture and storage: an overview. *Chemical Engineering Research and Design*, 89(9):1446–1460, 2011.

- [44] Klaas Van Alphen, Paul M Noothout, Marko P Hekkert, and Wim C Turkenburg. Evaluating the development of carbon capture and storage technologies in the united states. *Renewable and Sustainable Energy Reviews*, 14(3):971–986, 2010.
- [45] Jean-Michel Lemieux. The potential impact of underground geological storage of carbon dioxide in deep saline aquifers on shallow groundwater resources. *Hydrogeology Journal*, 19(4):757–778, 2011.
- [46] Paul Emeka Eke, Andrew Curtis, Stuart Haszeldine, et al. Co₂-brine surface dissolution and injection: Co₂ storage enhancement. In *Offshore Europe*. Society of Petroleum Engineers, 2009.
- [47] Dayong Wang, Bo Dong, Stephen Breen, Minglong Zhao, Juan Qiao, Yu Liu, Yi Zhang, and Yongchen Song. Approaches to research on co₂/brine two-phase migration in saline aquifers. *Hydrogeology Journal*, 23(1):1–18, 2015.
- [48] Holger Ott and Sjaam Oedai. Wormhole formation and compact dissolution in single-and two-phase co₂-brine injections. *Geophysical Research Letters*, 42(7):2270–2276, 2015.
- [49] Omer Izgec, Birol Demiral, Henri Bertin, and Serhat Akin. Co₂ injection into saline carbonate aquifer formations. *Transport in Porous Media*, 72(1):1–24, 2008.